DESIGN AND SIMULATION OF AIR CONDITIONING SYSTEM FOR LOCALLY BUILT BUS A CASE OF ISUZU FSR

Henok Mebratu Hailesilase

A Thesis Submitted to

The Department of Mechanical Systems and Vehicle Engineering

School Of Mechanical, Chemical and Materials Engineering

Presented in Partial Fulfillment of the Requirement for the Award of the Degree of Master of Science in Automotive Engineering

Office of Graduate Studies

Adama Science and Technology University

June, 2021GC

Adama, Ethiopia

DESIGN AND SIMULATION OF AIR CONDITIONING SYSTEM FOR LOCALLY BUILT BUS A CASE OF ISUZU FSR

Henok Mebratu Hailesilase

Advisor: Ramesh Babu Nallamothu (PhD)

A Thesis Submitted to

The Department of Mechanical Systems and Vehicle Engineering

School of Mechanical, Chemical and Materials Engineering

Presented in Partial Fulfillment of the Requirement for the Award of the Degree of Master of Science in Automotive Engineering

Office of Graduate Studies

Adama Science and Technology University

June, 2021GC

Adama, Ethiopia

DECLARATION

I hereby declare that this Master Thesis entitled "Design and Simulation of Air Conditioning System for Locally Built Bus A Case of ISUZU FSR" is my original work. That is, it has not been submitted for the award of any academic degree, diploma or certificate in any other university. All sources of materials that are used for this thesis have been duly acknowledged through citation.

_________________	_________________	_________________
Name of the student	Signature	Date

RECOMMENDATION

I, the advisor of this thesis, hereby certify that I have read the revised version of the thesis entitled “Design and Simulation of Air Conditioning System for Locally Built Bus A Case of ISUZU FSR” prepared under my guidance by Henok Mebratu submitted in partial fulfillment of the requirements for the degree of Master of Science in Automotive Engineering.

Therefore, I recommend the submission of revised version of the thesis to the department following the applicable procedures.

________________	________________	________________
Advisor	Signature	Date

APPROVAL PAGE

I, the advisor of the thesis entitled "Design and Simulation of Air Conditioning System for Locally Built Bus A Case of ISUZU FSR" and developed by Henok Mebratu, hereby certify that the recommendation and suggestions made by the board of examiners are appropriately incorporated into the final version of the thesis.

Advisor	Signature	Date

We, the undersigned, members of the Board of Examiners of the thesis by Henok Mebratu have read and evaluated the thesis entitled "Design and Simulation of Air Conditioning System for Locally Built Bus A Case of ISUZU FSR" and examined the candidate during open defense. This is, therefore, to certify that the thesis is accepted for partial fulfillment of the requirement of the degree of Master of Science in Automotive Engineering.

Chairperson	Signature	Date
Internal Examiner	Signature	Date
External Examiner	Signature	Date
Department Head	Signature	Date
School Dean	Signature	Date
Office of Postgraduate Studies, Dean	Signature	Date

ACKNOWLEDGEMENT

Above all, my utmost gratitude goes to the almighty God for his graciously provision of knowledge, wisdom and inspiration and he is always with me in all my day-to-day activities and giving me strength to complete this thesis.

My deepest and sincere appreciation also move to my advisor Dr. Ramesh Babu Nallamothu (Ph.D.) for his understanding, valuable comments, and professional advice from time of inception to the completion of this thesis.

I am also grateful to thank Ato Shumbeza Fikadu, Owner of Garage for his substantial support and provision with necessary information and materials.

Last but not least, I would like to thank my parents and friends for their supports and allowing me to fully focus myself on this thesis even on weekends.

ABSTRACT

Automotive air conditioning system is playing an important role in human thermal comfort, uniform temperature distribution and to some extent safety during vehicle driving in varied atmospheric conditions. Now a day there is competition between public long-distance bus transport companies in Ethiopia in providing comfortable, right on time, and enjoyable trip to any part of Ethiopia. But local body-built buses are not air conditioned and make your trip worst and exhausting. To make these buses more comfortable and competitive with other imported air-conditioned buses it is better to design effective air conditioning system locally based on the number of passengers, distance traveled, outdoor weather conditions, indoor design conditions, dimensions and optical properties of glass, dimensions and thermal properties of materials in bus body, and Power and torque limitations of bus engine. In this thesis work, Air conditioning system was designed based on passenger comfort parameters depending on working environment provided with air condition system of in the bus having passengers including the driver. Cooling load is analyzed by using Analytical methods based on ASHRAE for the Design and Application of Heating, Ventilation and Air Conditioning for Passenger Vehicles. Cooling load was calculated for 44 passengers of the ISUZU FSR bus, as per the calculations of cooling load obtained from the bus is 26.08 kW. With respect to the obtained results, air conditioning system was selected and designed. Then using ANSYS Fluent computational fluid dynamics (CFD) software the designed air conditioning system air flow and temperature distribution simulated to validate the design before building first to reduce the testing time and cost. CFD model incorporated with the combined SST $k-\omega$ *turbulence model and the results were checked against the aspect of "grid independence". Results of simulation shows the designed air conditioning system is capable of insuring satisfactory thermal conditions for the passengers.*

Keywords: Air conditioning, Thermal comfort, Computational Fluid Dynamics, ANSYS Fluent

TABLE OF CONTENTS

Contents page

ACRONYMS

A	Solar irradiation at air mass zero for each month
A_g	Area of glass
A_{eng}	Surface area exposed to the engine temperature
A_{exh}	Surface area exposed to the exhaust pipe temperature
AC	Air conditioning
ASHRAE	American Society of Heating, Refrigerating and Air conditioning Engineers
AST	Apparent solar time
B	Atmospheric extinction coefficient
C	Ratio of diffuse radiation on horizontal surface to direct normal irradiation
CFD	Computational fluid dynamics
$C_{\circ}$	Fitting pressure loss factor
C_p	Specific heat capacity
$SHGC$	Solar heat gain coefficient
$\langle SHGC \rangle_D$	Diffuse solar heat gain coefficient
ET	Equation of time
E_D	Direct irradiance
E_{DN}	Direct normal irradiance
E_{ds}	Diffuse sky irradiance
E_{dg}	Diffuse ground reflected irradiance
E_o	Extraterrestrial normal irradiance
H	Hour angle
HVAC	Heating, ventilation and air conditioning

h_{fg}	Latent heat of vaporization of water
h_i	Outdoor surface heat transfer coefficient
h_o	Outdoor surface heat transfer coefficient
k	Thermal conductivity
k_a	Air gap
LON	Longitude
LSM	Standard meridian longitude
LST	Local standard time
$\dot{m}_v$	Mass flow rate of ventilated air
p_v	Velocity pressure
$\dot{Q}_{c,g}$	Heat gain through glass by conduction and convection
$\dot{Q}_{con}$	Heat gain through bus body
$\dot{Q}_{s,b}$	Direct beam radiation load
$\dot{Q}_{s,d}$	Diffuse radiation load
$\dot{Q}_{engine}$	Heat gain from the engine
$\dot{Q}_{exhaust}$	Heat gain from exhaust
$\dot{Q}_{int}$	Internal object heat gain
$\dot{Q}_{pass}$	Heat from passenger
$\dot{Q}_{pass,s}$	Sensible heat gain due to passenger
$\dot{Q}_{pass,l}$	Latent heat gain due to passenger
$\dot{Q}_S$	Required bus heating or air conditioning system load
$\dot{Q}_{solar}$	Heat gain through glass by solar radiation
$\dot{Q}_v$	Ventilation load
$\dot{Q}_{v,s}$	Sensible heat gains due to ventilation

$\dot{Q}_{\mathrm{v,l}}$	Latent heat gains due to ventilation.
T_{eng}	Engine temperature
$T_{exhaust}$	Exhaust pipe side air temperature
T_i	Indoor temperature
T_o	Outdoor temperature
T_s	Surface temperature
TZ	Time zone
t	Time
UTC	Universal time coordinate
U_g	Overall heat transfer coefficient of the glass
U_j	Velocity in *j* direction
$\dot{V}$	Ventilation rate
v_a	Moist air specific volume
x_j	Distance in *j* direction
Y	Ratio of vertical/horizontal sky diffuse
α	Solar absorbance
θ	Angle of incidence
β	Altitude angle
γ	Surface-solar azimuth angle
ϕ	Solar azimuth
ψ	Surface azimuth
Σ	Surface tilt angle measured from the horizontal
τ	Surface element transmissivity
δ	Solar declination

ρ	Density
ρ_g	Reflectance of the foreground
Γ_ϕ	Generalized diffusion coefficient
ω_i	Indoor humidity ratio
ω_o	Outdoor humidity ratio
Δp	Pressure drops across fitting

LIST OF TABLES

LIST OF FIGURES

CHAPTER ONE

INTRODUCTION

1.1 Background

Air conditioning is the process of removing heat and moisture from the interior of an occupied space to improve the comfort of occupants. The air conditioning system is the device that helps us to achieve that. It can be installed in our house, office, cars, even a big modern factory now have it. In short, it can be used in both domestic and commercial environments. This process is most commonly used to achieve a more comfortable interior environment, typically for humans and other animals (Bhargava, 2020).

Heating, ventilation and air conditioning (HVAC) in automotive transport are not just a function of temperature control. The safety of occupants to reduce driver fatigue, ensure good visibility and maintain comfort is key to the successful design of such systems. The HVAC system creates a comfort zone for the occupants which can be adjusted within a range. Not all humans desire exactly the same environment, variations occur due to different continents, countries, cultures, gender, age or simply due to the type/amount of clothing being worn when inside the vehicle. The system must provide a way of controlling the climate inside the vehicle which is generally referred to as ‘climate control’.

Air-conditioning and heating systems for buses and rail cars generally use commercial components, but are packaged specifically for each application, often integral with the styling. Mass, envelope, power consumption, maintainability, and reliability are important factors. Power sources may be electrical, engine crankshaft, compressed air, or hydraulic. These sources are often limited, variable, and interruptible. Design aspects common to all mass-transit HVAC systems include passenger comfort (ventilation, thermal comfort, air quality, expectation) and thermal load analysis (passenger dynamic metabolic rate, solar loading, infiltration, multiple climates, vehicle velocity, and, in urban applications, rapid interior load change) (ASHRAE Handbook HVAC, 2019).

This thesis is mainly focus on a detailed analysis of the comfort parameters and improving thermal comfort by designing air conditioning system for locally body manufactured buses.

1.2 Statement of the problem

Nowadays there is competition between public long-distance bus transport service providing companies in Ethiopia by providing comfortable and enjoying your trip to any part of Ethiopia. The buses used to provide this service are almost all of them imported from abroad which causes the country to invest millions of Dollars. The passenger compartment of locally body-built buses is a narrow and enclosed space usually with a high population density. Due to long trip duration, thermal comfort becomes an essential factor to consider.

The locally built buses in Ethiopia are not equipped with air conditioning system making them not able to compete with imported buses in providing comfortable conditions for passengers. Due to this these buses are not able to attract the passengers for long trips making bus owner unprofitable.

1.3 Objectives of Study

1.3.1 General Objective

The general objective of this thesis is to design air conditioning system so that local bus body manufacturing companies can include such system in the future to increase passenger comfort.

1.3.2 Specific Objectives

The specific objectives are:

- To evaluate the cooling load under different operating conditions.
- To design and select the components of air conditioning.
- To simulate the design using ANSYS Fluent computational fluid dynamics (CFD) software.

1.4 Significance of the thesis

The significance of the thesis work is the following

- The results of this work can be applied to locally built buses.
- Makes local body-built bus more preferable and competitive over imported buses.

- Increase passenger comfort in public transport and keeps passengers healthier.
- Country gets benefitted financially due to reduction in importation of the buses.

1.5 Beneficiaries

Local bus body manufacturing companies or garages, vehicle owners, researchers, society and country as a whole get benefitted with this work.

1.6 Delimitation (Scope)

This thesis is limited to cooling load calculation and simulation of air conditioning system for buses, the bodies of which are manufactured in the country. Traditional vapor compression air conditioning system is taken into consideration not the vapor absorption system.

1.7 Organization of the thesis

This thesis is organized in to six chapters. The first chapter is the introductory part which is briefly introduce air conditioning system, statement of the problem, objectives, significance, beneficiaries, and scope of the study. Chapter 2 reviews the previous research works that were conducted by other people. This includes a general overview of bus air conditioning, human thermal comfort, and indoor airflow modeling. Chapter 3 contains details of methods used to compute the heat loads on the bus to provide total heat gained. Chapter 4 presents design and selections of bus air conditioning components. And briefly describes steps to simulate the inside of bus compartment. Chapter 5 details the simulation results of air circulation and temperature distribution inside passenger compartment and a discussion will be set up in this chapter. Chapter 6 which is the last chapter includes a summary of findings, conclude the results of this thesis study, and recommendation for future works.

CHAPTER TWO

LITERATURE REVIEW

2.1 Bus air conditioning system

In general, bus air-conditioning systems can be classified as interurban, urban, or small/shuttle bus systems. Bus air-conditioning design differs from other air-conditioning applications because of climatic conditions in which the bus operates, equipment size limitations, vehicle engine, electrical generator, and compressor rev/s. Providing a comfortable climate inside a bus passenger compartment is challenging because the occupancy rate per unit of surface and air recirculation volume is high, glazed area is very large, and outdoor conditions are highly variable. Factors such as high ambient temperatures, dust, rain, snow, road shocks, hail, and sleet should be considered in the design. Units should operate satisfactorily in ambient conditions from –30 to 50°C (ASHRAE Handbook HVAC, 2019).

2.1.1 Interurban buses

These buses are designed to accommodate up to 56 passengers. The air-conditioning system is usually designed to handle extreme conditions. Interurban buses produced in North America are likely to have the evaporator and heater located under the passenger compartment floor. A four- or six-cylinder reciprocating compressor, in which some cylinders are equipped with unloaders, is popular. Some interurban buses have a separate engine-driven compressor, preferably scroll, to give more constant system performance. Figure 2.1 shows a typical air-conditioning arrangement for an interurban bus.

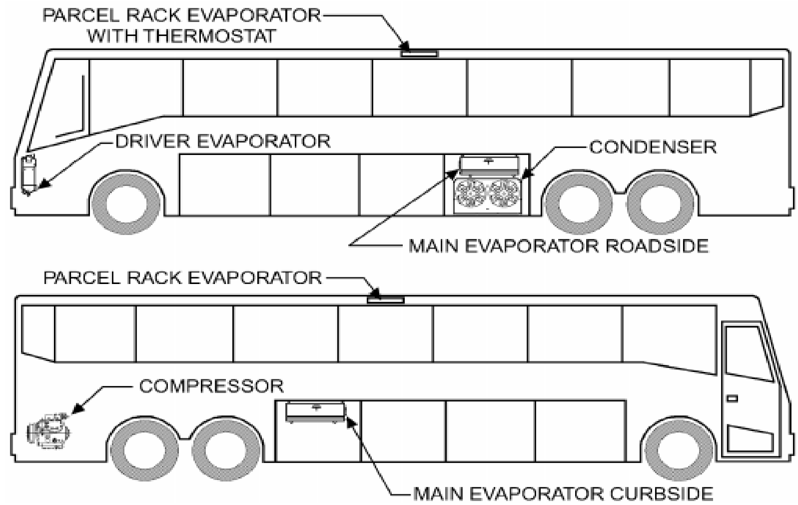

Figure 2.1. Typical arrangement of air conditioning in Interurban bus (ASHRAE Handbook HVAC, 2019)

2.1.2 Urban buses

Urban bus heating and cooling loads are greater than those of the interurban bus. A city bus may seat up to 50 passengers and carry a “crush load” of standing passengers. The fresh-air load is greater because of the number of door openings and the infiltration around doors. Cooling capacity required for a typical 50-seat urban bus is from 20 to 35 kW. The buses are usually equipped with a roof- or rear-mounted unit, as shown in Figure 2.2. One or two compressors are usually belt-or shaft-driven from the propulsion engine. Capacity control is very important, because the compressor may turn more quickly than necessary at high engine speeds. Therefore, capacity control must compensate for not only the thermal load but also the engine-induced load. Cylinder unloaders are the primary means of capacity control, although evaporator pressure regulators have been used with non-unloading compressors, as shown in

Figure 2.2. Low-profile, self-contained, rooftop-mounted units are used for urban and interurban buses. These units contain the entire air conditioning system except for the compressor, which is shaft- or belt-driven from the bus engine (see Figure 2.3).

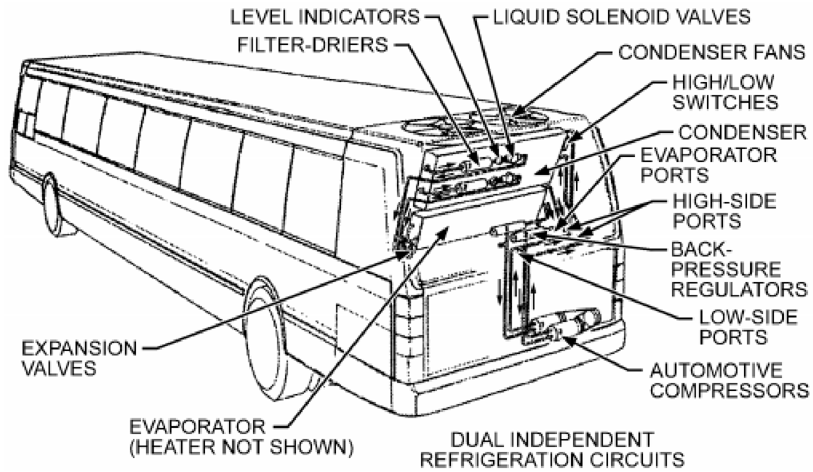

Figure 2.2. Typical mounting location of urban bus air conditioning equipment (ASHRAE Handbook HVAC, 2019).

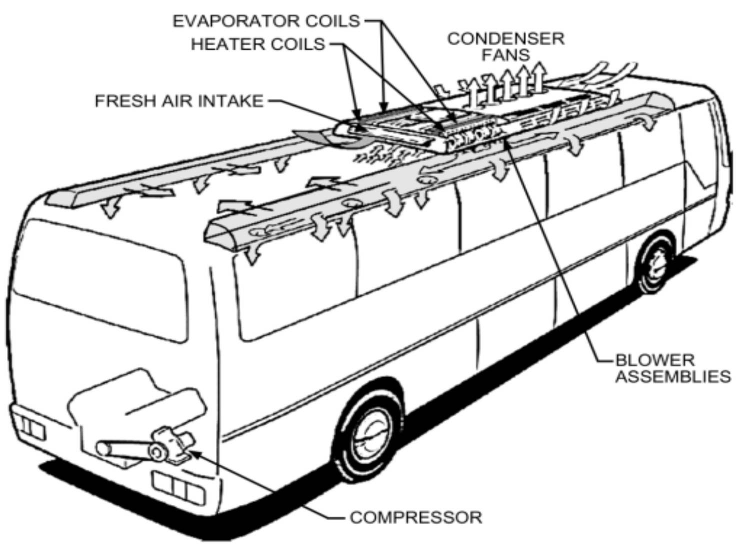

Figure 2.3. Typical mounting location of roof mounted urban bus air conditioning equipment with single compressor (ASHRAE Handbook HVAC, 2019).

2.1.3 Small or shuttle buses

For small or shuttle buses such as those typically operating around airports or for schools, the evaporator is usually mounted in the rear and the condenser on the side or the roof of the bus. The evaporator unit is typically a free-blow unit.

2.2 Human thermal comfort

Thermal comfort is the condition of mind which expresses satisfaction with the thermal environment and is assessed by subjective evaluation (ASHRAE Standard 55, 2017). The human body can be viewed as a heat engine where food is the input energy. The human body will release excess heat into the environment, so the body can continue to operate. The heat transfer is proportional to temperature difference. In cold environments, the body loses more heat to the environment and in hot environments the body does not release enough heat. Both the hot and cold scenarios lead to discomfort (Cengel and Boles, 2010). Maintaining this standard of the thermal comfort for occupant bus or other enclosures is one of the important goals of Air conditioning design engineers.

The heat balance of a human body is affected by six primary environmental and personal factors (ASHRAE Standard 55, 2017). The six primary factors are air temperature, air speed, relative humidity, mean radiant temperature, metabolic rate and clothing insulation.

- Air temperature: The air temperature is the average temperature of the air surrounding the occupant, with respect to location and time. The air temperature alone is one of the leading and most sensible factors for thermal comfort. Its change is able to easily manipulate the levels of perceptions for it in humans. Most people feel comfortable when the environment temperature is between 22 and 27°C (Cengel and Boles, 2010).

- Air speed: Air speed is the rate of air movement at a point, without regard to direction (ASHRAE Standard 55, 2017). Air motion also plays an important role in human comfort. It removes the warm, moist air that builds up around the body and replaces it with fresh air. Therefore, air motion improves heat rejection by both convection and evaporation. Air motion should be strong enough to remove heat and moisture from the vicinity of the body, but gentle enough to be unnoticed. Therefore, the designer shall decide the proper averaging, especially including air speeds incident on unclothed body parts, that have greater cooling effect and potential for local discomfort.

- Relative humidity: Relative humidity is the ratio of the amount of water vapor in the air to the amount of water vapor that the air could hold at the specific temperature and pressure (ASHRAE Standard 55, 2017). The relative humidity also has a considerable effect on comfort since it affects the amount of heat a body can dissipate through evaporation. High relative humidity slows down heat rejection by evaporation, and low relative humidity speeds it up. Most people prefer a relative humidity of 40 % to 60 %. Relative humidity values under 40% have been shown to cause eye and throat irritation, and drying of the mucous membranes and nasal passages while relative humidity values above 60% can cause reduced evaporative cooling of the body, mold growth in buildings and other moisture related problems (Cengel and Boles, 2010). The thermal comfort sensation is optimal when the relative humidity value is about 50% (ASHRAE Handbook Fundamentals, 2017).

- Mean radiant temperature: temperature is the temperature of a uniform, black enclosure that exchanges the same amount of heat by radiation with the occupant as the actual surroundings (ASHRAE Standard 55, 2017).

- Metabolic rate: Metabolic rate is the rate of transformation of chemical energy into heat and mechanical work by metabolic activities of an individual, per unit of skin surface area (expressed in units of met) equal to 58.2 W/m^2, which is the energy produced per unit skin surface area of an average person seated at rest (ASHRAE Standard 55, 2017).

  (ASHRAE Standard 55, 2017) provides a table of met rates for a variety of activities. Some common values are 0.7 met for sleeping, 1.0 met for a seated and quiet position, 1.2-1.4 met for light activities standing, 2.0 met or more for activities that involve movement, walking, lifting heavy loads or operating machinery. For intermittent activity, the Standard states that it is permissible to use a time-weighted average metabolic rate if individuals are performing activities that vary over a period of one hour or less. For longer periods, different metabolic rates must be considered.

- Clothing insulation: The amount of thermal insulation worn by a person has a substantial impact on thermal comfort, because it influences the heat loss and consequently the thermal balance. Layers of insulating clothing prevent heat loss and can either help keep a person warm or lead to overheating. Generally, the thicker the garment is, the greater insulating ability it has. Depending on the type of material the clothing is made out of, air movement and relative humidity can decrease the insulating ability of the material.

2.3 Climatic design condition

The climatic design condition provides information for those locations for long-term hourly observations were available (at least 10 years of data). The information includes design values of dry-bulb, wet-bulb, and dew-point temperature at various frequencies of occurrence. These data allow the designer to consider various operational peak conditions. This climatic design information is commonly used for design, sizing, distribution, installation, and marketing of heating, ventilating, and air-conditioning equipment (ASHRAE Handbook Fundamentals, 2017).

Warm-season temperature and humidity conditions are based on annual percentiles of 0.4, 1.0, and 2.5. Cold-season conditions are based on annual percentiles of 99.6, 99.0, and 97.5. The use of annual percentiles to define design conditions ensures that they represent the same probability of occurrence in any climate, regardless of the seasonal distribution of extreme temperature and humidity (ASHRAE Handbook Fundamentals, 2017).

Annual cooling design conditions contains information as follows:

- Hottest month (i.e., month with highest average dry-bulb temperature; 1 = January, 12 = December)
- Dry-bulb temperature corresponding to 0.4%, 1.0%, and 2.5% annual cumulative frequency of occurrence and the mean coincident wet-bulb temperature (warm), °C. This implies that 0.4%, 1.0%, and 2.5% of the time in a year, the outdoor air temperature will be above the design condition.
- Wet-bulb temperature corresponding to 0.4%, 1.0%, and 2.5% annual cumulative frequency of occurrence and the mean coincident dry-bulb temperature.
- Dew-point temperature corresponding to 0.4%, 1.0%, and 2.5% annual cumulative frequency of occurrence and the mean coincident dry-bulb temperature and the humidity ratio (calculated for the dew-point temperature at the standard atmospheric pressure at the elevation of the station).
- Mean daily range for hottest month, °C (defined as mean of the difference between daily maximum and daily minimum dry-bulb temperatures for hottest month).

Values of ambient dry-bulb, dew-point, and wet bulb temperature corresponding to the various annual percentiles represent the value that is exceeded on average by the indicated percentage of the total number of hours in a year (8760). The 0.4%, 1.0%, and 2.5% values are exceeded on average 35, 88, and 219 h per year, respectively, for the period of record. Mean coincident values are the average of the indicated weather element occurring concurrently with the corresponding design value. These design conditions were calculated from the frequency distribution analyzed from data sets observed over several years (EBCS-11, 2014).

These design conditions were calculated from the frequency distribution analyzed from data sets observed over several years. Although the minimum period of record selected for this analysis was 10 years, some variation and gaps in observing programs meant that some months' data were unusable due to incompleteness (EBCS-11, 2014).

2.4 Indoor airflow modeling

When trying to determine best design practice for specific indoor spaces, designers may encounter uncertainties regarding control of airflow, indoor air quality, thermal comfort, or heat transfer. Evaluating performance of complex and highly engineered designs is often beyond the ability of the tables, rules of thumb, and simple formula given in the handbooks. In these situations, computer models allow designers to quantitatively evaluate multiple designs quickly and with a good degree of accuracy (ASHRAE Handbook HVAC, 2019).

2.4.1 Computational fluid dynamics

Computational fluid dynamics (CFD) is a branch of fluid mechanics that uses numerical analysis and data structure to analyze and solve problems that involves fluid flows. CFD methods simulate the detailed airflow distribution and related physical phenomena in a space and provide detailed information, such as temperature at specific points. However, due to the relatively high computational cost, the size and geometric complexity of the space that can be modeled is limited by the computational resource available. Practitioners who plant to use CFD must weigh the computational requirement against the expected accuracy of the simulated results to determine the appropriate level of detail to implement in the CFD model (ASHRAE Handbook HVAC, 2019).

CFD involves solving coupled partial differential equations, which must be worked simultaneously or successively. No analytical solutions are available for indoor environment modeling. Computer based numerical procedures are the only means of generating complete solutions of these sets of equations.

CFD code is more than just a numerical procedure of solving governing equations; it can be used to solve fluid flow, heat transfer, chemical reactions, and even thermal stresses. Unless otherwise implemented, CFD does not solve acoustics and lighting, which are also important parameters in indoor environment analysis. Different CFD codes have different capabilities: a simple code may solve only laminar flow, whereas a complicated one can handle a far more complex flow (ASHRAE Handbook Fundamentals, 2017).

2.4.1.1 Geometry generation

A physical model of the specific space to be modeled in the CFD simulation is generated from the scratch or converted from an existing model. Whether the geometry includes both the fluid and solid portion depends on the scope of the analysis. The geometric model should capture all essential features of the space such as flow obstructions equipment air supply/return devices, and heat sources (e.g., exterior glazing, occupants, equipment). The geometric model should be kept as simple as possible, while still maintaining sufficient accuracy and satisfying the intent of the analysis (ASHRAE Handbook HVAC, 2019).

2.4.1.2 Meshing for computational fluid dynamics

Meshing is an integral part of the engineering simulation process where complex geometries are divided into simple elements that can be used as discrete local approximations of the larger domain. The mesh influences the accuracy, convergence and speed of the simulation. Furthermore, since meshing typically consumes a significant portion of the time it takes to get simulation results, the better and more automated the meshing tools, the faster and more accurate the solution. Mesh creation may be occurred in or outside of the CFD software package (ASHRAE Handbook HVAC, 2019).

Meshes can be structured or unstructured, depending on the connectivity of the cells in the mesh to one another. Individual cell shape varies, and each shape has advantages and disadvantages.

These shapes range from triangles and quadrilaterals for two-dimensional (2D) geometry, to tetrahedral (four-sided triangular based shapes) and hexahedrons (typically six-sided boxes) for three-dimensional (3D) geometry. Wedges (a triangle swept into a three-dimensional shape) and rectangular-based pyramids can also be used to transition between the triangular sides of the tetrahedra's and quadrilateral sides of the hexahedrons (ASHRAE Handbook Fundamentals, 2017).

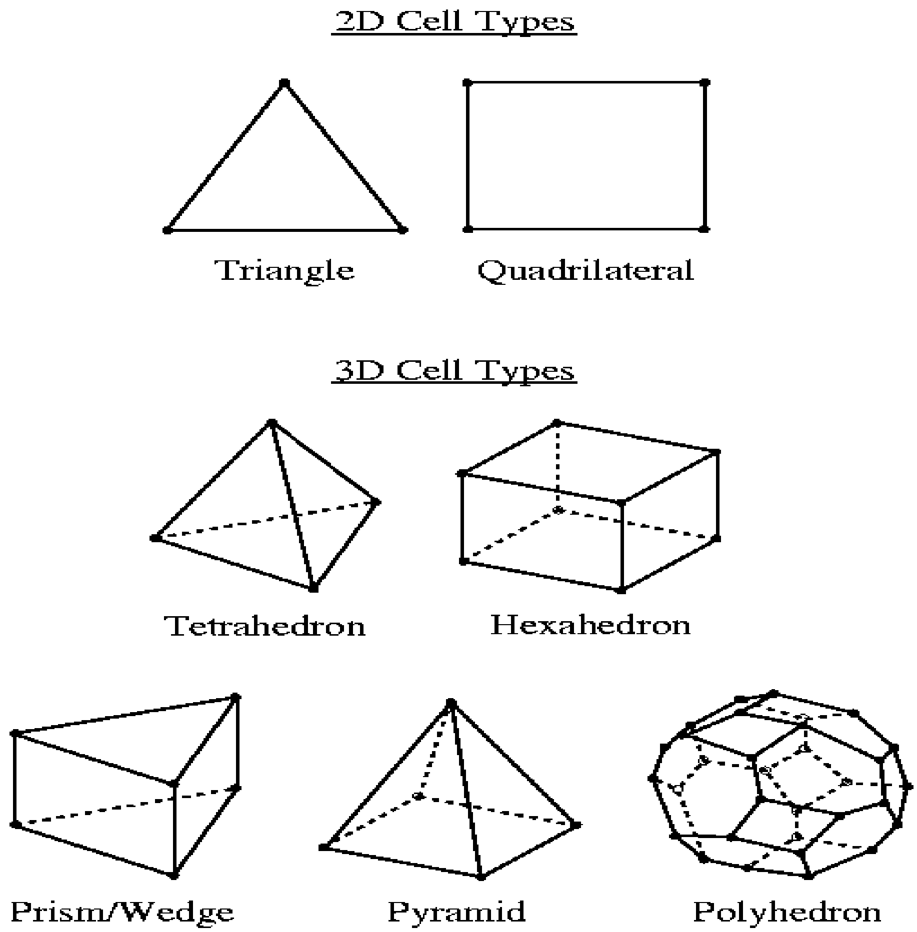

Figure 2.4. Basic two and three-dimensional cell types (ANSYS Fluent 12.0, 2009)

2.4.1.3 Governing equations in computational fluid dynamics

Indoor airflow, convective heat transfer, and species dispersion are controlled by the governing equations for mass, momentum in each flow direction, energy, and contaminant distribution. Continuity equations, Navier-Stokes equations and energy equations are the key governing equations that dictate the physics of fluid mechanics and thermal sciences, which are instrumental in the research of computational fluid dynamics. The governing equations in this study are Navier-Stokes equations. A common form is presented in Equation 2.1, relating the change in time of a variable at a location to the amount of variable flux (e.g., momentum, mass, thermal energy). Essentially, transient changes plus convection equals diffusion plus sources (ASHRAE Handbook Fundamentals, 2017):

$$\frac{\partial}{\partial t}(\rho\phi) + \frac{\partial}{\partial x_j}\left(\rho U_j \phi\right) = \frac{\partial}{\partial x_j}\left(\Gamma_\phi \frac{\partial \phi}{\partial x_j}\right) + S_\phi \qquad 2.1$$

Where t is time in seconds, ρ is density, ϕ is transport property (e.g., air velocity, temperature, species concentration) at any point, x_j is distance in *j* direction, U_j is velocity in *j* direction, Γ_ϕ is generalized diffusion coefficient or transport property of fluid flow.

2.4.1.4 Turbulence modelling

One of today's most important challenge for the numerical solution of fluid flow problems is the modeling and simulation of turbulence. Airflow in natural and built environments is predominantly turbulent, characterized by randomness, diffusivity, dissipation, and relatively large Reynolds numbers. Turbulence is not a fluid property, as are viscosity and thermal conductivity, but a phenomenon caused by flow motion (ASHRAE Handbook HVAC, 2019).

Turbulent flows are characterized by fluctuating velocity fields. These fluctuations mix transported quantities such as momentum, energy, and species concentration, and cause the transported quantities to fluctuate as well. Since these fluctuations can be of small scale and high frequency, they are too computationally expensive to simulate directly in practical engineering calculations. Instead, the instantaneous (exact) governing equations can be time-averaged, ensemble-averaged, or otherwise manipulated to remove the resolution of small scales, resulting in a modified set of equations that are computationally less expensive to solve. However, the modified equations contain additional unknown variables, and turbulence models are needed to determine these variables in terms of known quantities. There is no single model is considered to be superior for all types of applications. Some of the turbulence models that are mainly used are discussed below (ANSYS Fluent 12.0, 2009).

A. K-epsilon $\boldsymbol{k - \mathcal{E}}$ models

K-epsilon $k - \mathcal{E}$ turbulence model is the most common model used in CFD to simulate mean flow characteristics for turbulent flow conditions. It is a two equation model that gives a general description of turbulence by means of two transport equations. The original impetus for the K epsilon model was to improve the mixing-length model, as well as to find an alternative to algebraically prescribing turbulent length scales in moderate to high complexity flows. The first transported variable is the turbulent kinetic energy k.The second transported variable is the rate of dissipation of turbulent kinetic energy $\mathcal{E}$ (ANSYS Fluent 12.0, 2009).

Standard $\boldsymbol{k-\mathcal{E}}$ model: is a semi-empirical model, and the derivation of the model equations relies on phenomenological considerations and empiricism. Standard $k-\mathcal{E}$ model is a semi-empirical model based on model transport equations for the turbulence kinetic energy (k) and its dissipation rate ($\mathcal{E}$). The model transport equation for k is derived from the exact equation, while the model transport equation for $\mathcal{E}$ was obtained using physical reasoning and bears little resemblance to its mathematically exact counterpart.

RNG $\boldsymbol{k-\mathcal{E}}$ model: is derived from the instantaneous Navier-Stokes equations, using a mathematical technique called "renormalization group" (RNG) methods. It is similar in form to the standard $k-\mathcal{E}$ model, but includes the following refinements:

- The RNG model has an additional term in its $\mathcal{E}$ equation that significantly improves the accuracy for rapidly strained flows.
- The effect of swirl on turbulence is included in the RNG model, enhancing accuracy for swirling flows.
- The RNG theory provides an analytical formula for turbulent Prandtl numbers, while the standard $k-\mathcal{E}$ model uses user-specified, constant values.

Realizable $\boldsymbol{k-\mathcal{E}}$ model: is a relatively recent development and differs from the standard $k-\mathcal{E}$ model in two important ways:

- The realizable $k-\mathcal{E}$ model contains a new formulation for the turbulent viscosity.
- A new transport equation for the dissipation rate, $\mathcal{E}$, has been derived from an exact equation for the transport of the mean-square vorticity fluctuation.

The term "realizable" means that the model satisfies certain mathematical constraints on the Reynolds stresses, consistent with the physics of turbulent flows. Neither the standard $k-\mathcal{E}$ model nor the RNG $k-\mathcal{E}$ model is realizable.

B. K-omega ($\boldsymbol{k-\omega}$)models

The K-omega model is one of the most commonly used turbulence models. It is a two equation model, that means, it includes two extra transport equations to represent the turbulent properties of the flow. This allows a two equation model to account for history effects like convection and diffusion of turbulent energy (ANSYS Fluent 12.0, 2009).

The first transported variable is turbulent kinetic energy, k. The second transported variable in this case is the specific dissipation, ω. It is the variable that determines the scale of the turbulence, whereas the first variable, k, determines the energy in the turbulence.

Standard $\boldsymbol{k-\omega}$ model: The standard $k-\omega$ model is based on the Wilcox $k-\omega$ model, which incorporates modifications for low-Reynolds-number effects, compressibility, and shear flow spreading. The Wilcox model predicts free shear flow spreading rates that are in close agreement with measurements for far wakes, mixing layers, and plane, round, and radial jets, and is thus applicable to wall-bounded flows and free shear flows.

Shear-stress transport (SST) $\boldsymbol{k-\omega}$ model: SST $k-\omega$ model is a widely used and robust two-equation eddy-viscosity turbulence model used in CFD. The model combines the k-omega turbulence model and K-epsilon turbulence model such that the k-omega is used in the inner region of the boundary layer and switches to the k-epsilon in the free shear flow.

2.4.1.5 Boundary condition

Every surface in the CFD model provides a parameterized boundary to the fluid space that is simulated, and the conditions/inputs for these surfaces must be set. Several common boundaries typically encountered in indoor airflow simulations are as follows (ASHRAE Handbook Fundamentals, 2017).

- Wall: For most CFD software packages, any defined solid/ surface has the default classification of wall, which usually indicates a solid, non-permeable, no-slip surface. A wall can be slip or nonslip and/or have a roughness parameter associated with the surface, which can affect the turbulence simulation in the fluid region. In the case of the solid interacting with the fluid in a simulation, additional mechanisms may be introduced at the wall boundary. The interaction might include heat transfer, mass transfer, and chemical reactions.

- Inlet: A surface set to inlet classification allows fluid flow into the simulation domain. The property of this flow can be defined by its velocity, direction, pressure, or flow rate. In the case of multiphase or multicomponent fluid simulation, the inlet definition might include the exact mixture of the fluid.
- Outlet: This type of boundary allows fluid flow out of the simulation domain. Unlike an inlet, this boundary often does not require variables to be defined, because flow exiting the outflow boundary is outside of the simulation domain.
- Source: Source allow the specification of a flux of a specific quantity of interest. In most simulations, energy source of the domain might be specified as a heat flux on a given surface or volume. In a multispecies simulation, injection or removal of gas or particles are treated as mass flux. When a mechanism that impacts the flow field is needed, artificial momentum flux might be applied.

2.5 Literature reviews of prior studies supporting this thesis work

Andre et al. (1994) developed computational model for the purpose of simulating the behavior of the air conditioning system used in the bus passenger compartment. The model is based on the space integral energy balance equation for the air inside and for the main vehicle bodies and surfaces. In this paper, a space integral model capable of simulating the thermal behavior of various parts of a passenger bus is presented. It may be used as an aid tool in the project of heating and air conditioning system of the bus.

Ingersoll et al. (1992) developed a simple method to calculate passenger compartment thermal comfort. They calculated the thermal comfort of each vehicle occupant as a function of the prevailing local passenger compartment conditions of air temperature, mean radiant temperature, air velocity, air relative humidity, direct solar flux as well as the level of activity and clothing type of each individual. The availability of such method expected to aid the automotive engineers in the evaluation and selection of vehicle design parameters so as to optimize human comfort.

Vollaro (2013) studied indoor climate in city busses numerically and experimentally by creating a CFD model of a full cabin and validating the model with comparing the numerical and experimental methods. The numerical simulation results were experimentally validated by several measurements inside the urban buses performed under real operative conditions during the summer season. The numerical results obtained by CFD are in good agreements with experimental measurements (air temperature and speed). The model developed useful to predict the comfort results related with some new proposal in air conditioning, and grid distributions.

Berlitz and Matschke (2004) studied interior airflow simulation of a regional train. The CFD software used was ANSYS Fluent, with a standard $k - \mathcal{E}$ turbulence model. The interior airflow in a regional train first class compartment was simulated numerically. Thermodynamic and aerodynamic parameters were measured in a full-scale test train for the validation. The results show the capability of CFD for parameter variations and the prediction of thermal comfort.

Yongson et al. (2007) studied air flow analysis of an air conditioning room. They used standard $k - \mathcal{E}$ turbulence model for turbulent air flow modeling. They investigated different locations of blower placement to analyze for better comfort of occupant in the room. The results of simulation showed that the occupants will experience most comfort if the air conditioner blower is placed on the very corner of the side wall compared to the other locations. This work can also be extended to a more complex air conditioning system like in the industries and hospital.

Petrone et al. (2008) investigated the conditioning air distribution in a touring bus cabin. COMSOL Multi-physics is used as a powerful design and optimization tool for air distribution devices. The bus model is this analysis used two rows of seats with four passengers. In order to solve dynamical and thermal field in the considered air volume, momentum and energy equations have been solved adopting a $k - \mathcal{E}$ scheme for turbulence modelling. Results show that combining a standard ceiling system with a displacement scheme for the air inlets represents the best compromise for guaranteeing thermal comfort for passengers.

You et al. (2018) investigation proposed an innovative ventilation system that would reduce contaminant transport and maintain comfort for one row section of a fully occupied Boeing-737 cabin. Proposed ventilation system manufactured and installed in an occupied seven-row, single aisle cabin mockup. Air velocity, air temperature, and contaminant distribution in the cabin mockup were obtained by experimental measurements. The CFD model is solved using ANSYS Fluent with a hybrid turbulence model. this hybrid model uses the standard k-ω model in the near wall region and a transformed RNG k-ε model in the bulk air region. The conducted CFD simulation of the air distributions in the mockup and the experimental data was used to validate the CFD results. Results presented in this paper show the accuracy of the CFD simulation was acceptable for designing the cabin airflow.

Khayyam et al. (2009) studied about energy management system to reduce the energy consumption of a vehicle when its air conditioning system is in use by controlling the mass flow rate of the air dynamically adjusting the blower speed and air-gates opening under various loads. The results of study show vehicle comfort temperature achieved for reduced amount consumption.

Summary of literature review

The previous related work studied that the different thermal load analysis methods and CFD simulation. There are number of papers available in thermal load analysis but very few papers are available related vehicle air conditioning. The methodologies used by different authors are partially difficult to understand. As seen from the literature review above, there is no study that predicts the cooling load of locally body-built buses. Because of this, the present work mainly committed to calculate the cooling load at extreme hot location and simulation of air and temperature using ANSYS Fluent CFD software. In this study, the temperature distribution inside a long-distance bus cabin is investigated using numerical methods, similar to the studies mentioned in the literature review. During load calculations simplified and recent methods are used, and also easy to readers understand.

CHAPTER THREE

MATERIALS AND METHODS

3.1 Methods

The methodology followed in achieving the set objectives, includes various stages as briefly described below. It is shown in the form of a flowchart in Figure 3.1 below.

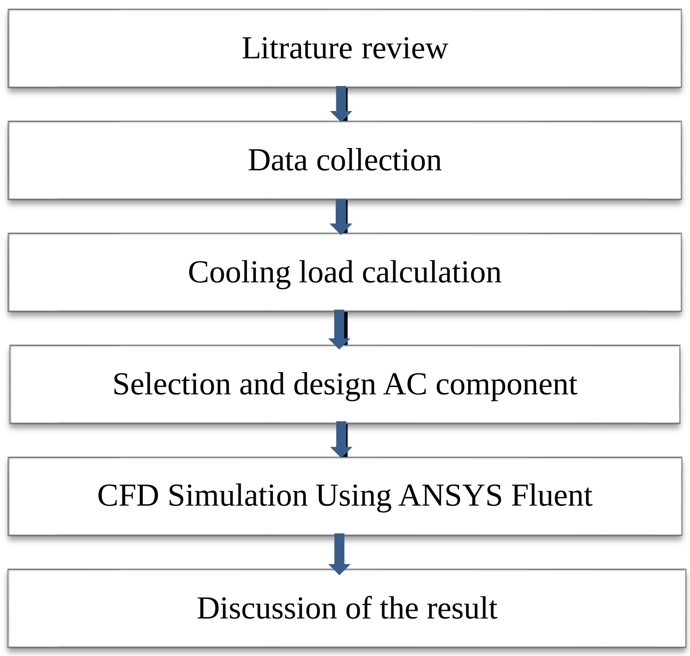

Figure 3.1. Methods

3.2 Literature review

Literature survey of the existing vehicle air conditioning system and the previous works related to bus air conditioning system design and simulation is the key step of the methodology which helps in gaining enough knowledge and helps in understanding the current status of the research in the field.

3.3 Methods of data collection

The necessary data for the cooling load calculation is collected by the following methods.

- By visiting local bus body manufacturing industries or garages and interaction with resource persons in the garage.
- By visiting various websites in the area of bus air conditioning design and simulation.

3.4 Thermal load analysis

Thermal load analysis for transit applications different from stationary, building based systems because vehicle orientation and occupant density changes regularly on street-level and long-distance transportation. summer operation is particularly affected because cooling load is affected more by solar and passenger heat gain than by outdoor air condition. For these reason, thermal loads must be calculated differently. Because buses must operate in various parts of the country, the air conditioning must be designed to handle the national seasonal extreme design days (ASHRAE Handbook HVAC, 2019).

The cooling load is the most difficult load to handle; the heating load is normally handled by heat recovered from the engine, external heater, or electrical heat elements.

There are different cooling and heating load calculation methods in practice. Among these, the heat balance and radiant time series methods are the dominant ways of analyzing load condition. The preferable one of the two methods is the heat balance method (EBCS-11, 2014).

The heat balance method is used for estimating the cooling or heating loads which develops inside the bus. To use the Heat Balance Method to analyze the net amount of heat added to bus the individual sources that add or remove heat from the space in question need to be identified. The Figure 3.2 shows schematically the various thermal load categories come across in a typical bus. The heat balance equation of the air inside bus passenger compartment is the following one (Andre et al., 1994):

$$\dot{Q}_{solar} + \dot{Q}_{c,g} + \dot{Q}_{con} + \dot{Q}_{engine} + \dot{Q}_{exhaust} + \dot{Q}_{pass} + \dot{Q}_{v} + \dot{Q}_{int} + \dot{Q}_{S} = 0 \qquad 3.1$$

Where $\dot{Q}_{solar}$ is heat gain through glass by solar radiation, $\dot{Q}_{c,g}$ is heat gain through glass by conduction and convection, $\dot{Q}_{con}$is heat gain through the bus body, $\dot{Q}_{engine}$is heat gain from the engine, $\dot{Q}_{exhaust}$ is heat gain from the exhaust, $\dot{Q}_{pass}$ is heat from passenger, $\dot{Q}_{v}$ is ventilation load, $\dot{Q}_{int}$ is heat gain from internal objects, and $\dot{Q}_{S}$ is the required bus heating or air conditioning system load.

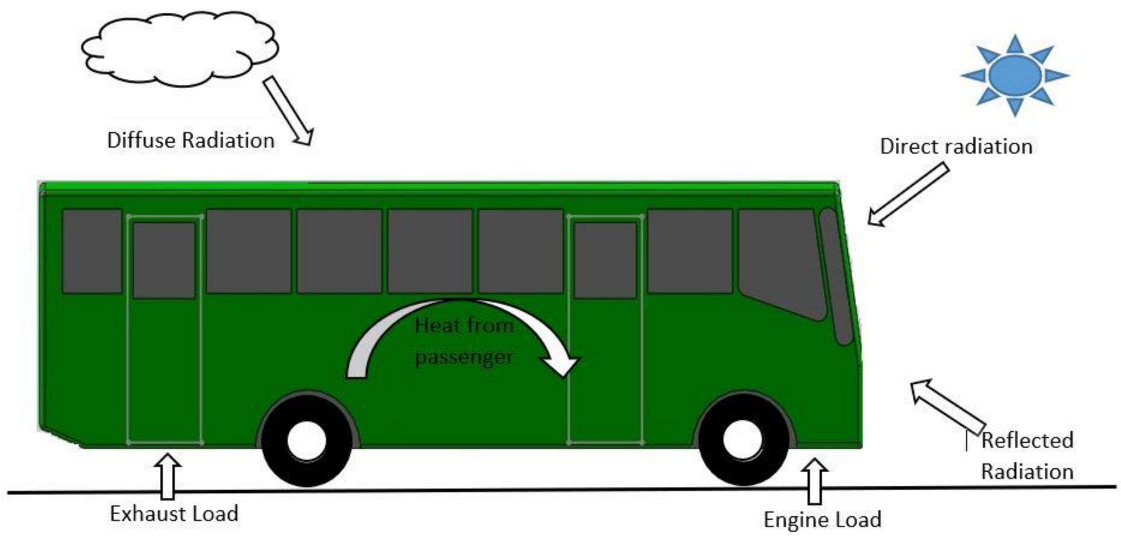

Figure 3.2. Schematic representation of thermal loads in a typical bus cabin

To calculate cooling load, detailed bus design information and weather data at selected design conditions are required.

To do the cooling load calculation first, the most extreme hot climate location was selected which the bus pass through or stay during its journey. The data from the Ethiopian National meteorology Agency, Ethiopian building code standard (EBCS 11, 2014), and different websites, Semera is the hottest location. Recommended outdoor design conditions for air conditioning applications in Semera are given in Table 3.1.

Table 3.1. Climatic design condition of Semera

Location/ City/Town	Semera, Afar
Latitude	11° 30'N
Longitude	41° 12'E
Elevation	633 m
Dry Bulb Temperature, DBT	44.5°C
Coincident Wet Bulb Temperature, CWB	28.71°C
Dew Point Temperature, DPT	21.81°C
Mean Daily Range, MDR	25.85°C
Hottest day of the year	June 13
Hottest hour	2:30 PM, 14:30, 14.5 hour
Time zone	UTC+03:00

After selecting most extreme hot climate location, the bus model was selected from local body manufacturer. The vehicle selected for AC design is ISUZU FSR, because the vehicle is the most popular and widely used in the country. A detailed description of the bus used for the field measurement is given in Table 3.2. Schematic diagram of the bus showing the dimensions is shown in Figure 3.3.

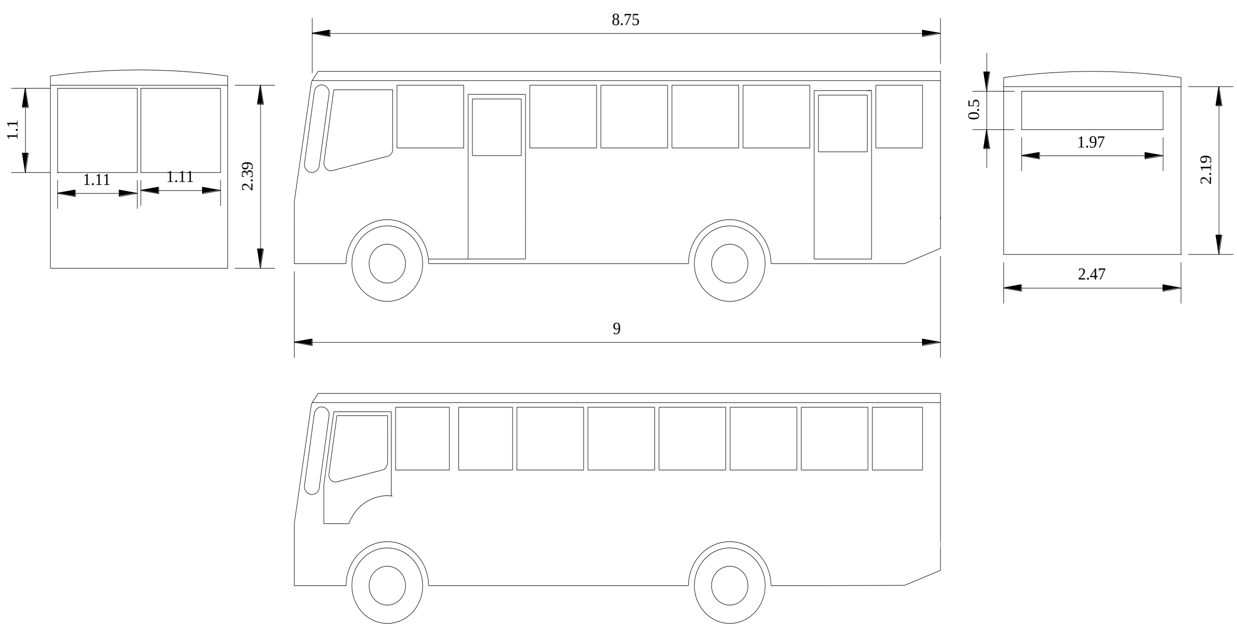

Figure 3.3. Schematic view and dimensions of ISUZU FSR bus

Table 3.2. Vehicle specification

Make			ISUZU FSR Bus	
Length, L			9 m	
Width, W			2.47 m	
Height, H			2.39 m	
Seating capacity			Driver + 44 Persons	
Maximum output, (hp/rpm)			175/ 2,850	
Speed of the bus			100 km/h = 27.78 m/s (max)	
	Area m^2	Material	Thickness(mm)	Thermal conductivity *k* (W/m.k)
Left hand side panel	13.8412	Sheet metal	1.25	50.2
		Air gap	40	0.024
		Sheet metal	1	50.2
Right hand side panel	13.7966	Sheet metal	1.25	50.2
		Air gap	40	0.024
		Sheet metal	1	50.2
Front panel	3.4613	Sheet metal	1.25	43
		Air gap	40	0.024
		Sheet metal	1	50.2
Back panel	4.4243	Sheet metal	1.25	50.2
		Air gap	40	0.024
		Sheet metal	1	50.2
Roof	21.6125	Sheet metal	1.25	50.2
		Air gap	120	0.024
		PVC	2.5	0.19
Floor	21.15	Sheet metal	2	50.2
Windshield	2.442		5	0.8
Back glass	0.985		4	0.8
Left hand side glass	6.3645		4	0.8
Right hand side glass	6.4091		6	0.8

Indoor design condition suggested by ASHRAE standard 55-2004 for thermal comfort purposes temperature could range from between 19.44°C to 27.78°C. for Summer conditions at 50% relative humidity optimum temperature of 24.5°C with an acceptable range of 23.5°C - 27.78°C.

3.4.1 Heat gain through glass by solar radiation

The glazing solar heat gain can be split into that beam radiation load ($\dot{Q}_{s,b}$) and diffuse radiation load ($\dot{Q}_{s,d}$), which includes both diffuse sky radiation and radiation scattered(reflected) from the ground (ASHRAE Handbook Fundamentals, 1997):

$$\dot{Q}_{solar} = \dot{Q}_{s,b} + \dot{Q}_{s,d} \tag{3.2}$$

Where $\dot{Q}_{s,b}$ is direct beam radiation load and $\dot{Q}_{s,d}$ is diffuse radiation load.

Beam radiation is that part of the incident solar radiation which directly strikes a surface of the vehicle glass, which is calculated from (ASHRAE Handbook Fundamentals, 1997; 2017):

$$\dot{Q}_{s,b} = SHGC\ A_g E_D \tag{3.3}$$

Where $SHGC$ is solar heat gain coefficient, A_g is the surface area of the glass, and E_D is the direct irradiance.

The direct irradiance is obtained from (ASHRAE Handbook Fundamentals, 1997):

$$E_D = E_{DN} \cos\theta \tag{3.4}$$

Where E_{DN} is the direct normal irradiance and θ is the angle between the surface normal and the position of sun in the sky.

The value of E_{DN} at surface of the earth on a clear day is represented by (ASHRAE Handbook Fundamentals, 1997):

$$E_{DN} = \frac{A}{\exp\left(\frac{B}{\sin\beta}\right)} \tag{3.5}$$

Where A is apparent solar irradiation at air mass zero for each month, B is atmospheric extinction coefficient, and β is the altitude angle that is calculated based on position and time.

The values of *A* and *B* vary during the year because of seasonal changes in the dust and water vapor content of the atmosphere, and also because of the changing earth- sun distance. The variations in values *A* and *B* Are listed in Table 3.3.

Table 3.3. Extraterrestrial solar irradiance and related data (ASHREA Handbook Fundamentals, 1997)

	I_o, W/m^2	Equation of time, min	Declination, degree	A W/m^2	B (Dimensionless Ratios)	C
Jan	1416	-11.2	-20.0	1230	0.142	0.058
Feb	1401	-13.9	-10.8	1215	0.144	0.060
Mar	1381	-7.5	0.0	1186	0.156	0.071
Apr	1356	1.1	11.6	1136	0.180	0.097
May	1336	3.3	20.0	1104	0.196	0.121
June	1336	-1.4	23.45	1088	0.205	0.134
July	1336	-6.2	20.6	1085	0.207	0.136
Aug	1338	-2.4	12.3	1107	0.201	0.122
Sep	1359	7.5	0.0	1151	0.177	0.092
Oct	1380	15.4	-10.5	1192	0.160	0.073
Nov	1405	13.8	-19.8	1221	0.149	0.063
Dec	1417	1.6	-23.45	1233	0.142	0.057

Glazing solar heat gain caused by diffuse incident radiation is calculated from (ASHRAE Handbook Fundamentals, 1997):

$$\dot{Q}_{s,d} = \langle SHGC \rangle_D \, A_g \, (E_{ds} + E_{dg}) \qquad 3.6$$

Where $\langle SHGC \rangle_D$ is diffuse solar heat gain coefficient, E_{ds} is diffuse sky irradiance, and E_{dg} is diffuse ground reflected irradiance.

The diffuse solar radiation from a clear sky that falls on any surface is given by Equation 3.7 and Equation 3.9 (ASHRAE Handbook Fundamentals, 1997; 2017).

For vertical surfaces,

$$E_{ds} = C \, Y \, E_{DN} \qquad 3.7$$

$$Y = \max(0.45,\ 0.55 + 0.437 \cos\theta + 0.313\, cos^2\, \theta \qquad 3.8$$

Surfaces other than vertical,

$$E_{ds} = C\, E_{DN}\, \left(\frac{1 + \cos\Sigma}{2}\right) \tag{3.9}$$

Where C is ratio of diffuse radiation on horizontal surface to direct normal irradiation, Y is ratio of vertical/horizontal sky diffuse, and Σ is the surface tilt angle measured from the horizontal surface.

Ground reflected irradiance for surfaces of all orientations is given by (ASHRAE Handbook Fundamentals, 1997):

$$E_{dg} = E_{DN}(C + \sin\beta)\rho_g\, \left(\frac{1-\cos\Sigma}{2}\right) \tag{3.10}$$

Where ρ_g *is* reflectance of the foreground and Σ is the surface tilt angle measured from the horizontal surface.

In order to estimate the heat gains due to solar radiation, it is necessary to set forth the relations among the sun, earth, locality, time of the day, and orientation. It is also necessary to establish the amount of direct and diffuse solar radiation received by the earth's surface with respect to various orientation.

Solar radiation at various times of year and day is required by several calculation methods for heat gains in air conditioning loads. To calculate solar radiation load first, we need to calculate solar angles for vehicle surfaces.

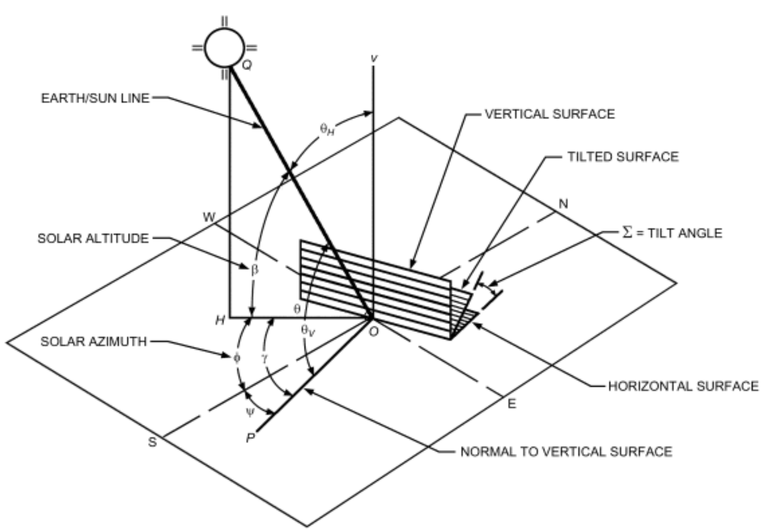

Figure 3.4. Solar angles for vertical and horizontal surface (ASHRAE Handbook Fundamentals, 2017).

The earth's orbital velocity also varies throughout the year, so apparent solar time (AST), as determined by a solar time sundial, varies somewhat from the mean time kept by a clock running at a uniform rate. This variation is called the equation of time (ET) and is approximated by the following formula (ASHRAE Handbook Fundamentals, 2017):

$$ET = 2.2918[0.0075 + 0.1868\cos(\Gamma) - 3.2077\sin(\Gamma) - 1.4615\cos(2\Gamma) - 4.089\sin(2\Gamma)] \quad 3.11$$

with ET expressed in minutes and

$$\Gamma = 360^0 \frac{n-1}{365} \quad 3.12$$

Where *n* is year day, with January 1 = 1. For June 13 at Semera *n* =164, so

$$\Gamma = 360^0 \frac{164-1}{365} = 160.77^0$$

$$ET = 2.2918[0.0075 + 0.1868\cos(160.77) - 3.2077\sin(160.77) - 1.4615\cos(2x160.77) - 4.089\sin(2x160.77)]$$

$$ET= 0.397^0 = 23.82 \text{ min}$$

Most standard meridians are found every 15° from 0° at Greenwich, U.K Standard meridian longitude is related to time zone as follows (ASHRAE Handbook Fundamentals, 2017):

$$LSM = 15TZ \quad 3.13$$

where TZ is the time zone, expressed in hours ahead or behind coordinated universal time (UTC). So, Semera time zone 3 hours ahead of UTC (UTC + 03:00).

$$LSM = 15(+3) = 45^0$$

The conversion between local standard time and solar time involves two steps: the equation of time is added to the local standard time, and then a longitude correction is added. This longitude correction is four minutes of time per degree difference between the local (site) longitude and the longitude of the local standard meridian (LSM) for that time zone; hence, AST is related to the local standard time (LST) as follows (ASHRAE Handbook Fundamentals, 2017):

Apparent Solar Time (AST) to Local Standard Time (LST) as follows:

$$AST = LST + ET/60 + (LON - LSM)/15 \quad 3.14$$

Where LST is local standard time (decimal hours) and LON is local longitude (degrees of arc)

Equation 3.13 leads to

$$\text{AST} = 14.5 + 23.82/60 + (41.12 - 45)/15 = 14.64h$$

The hour angle *H* defined as the angular displacement of the sun east or west of the local meridian due to the rotation of the earth, and expressed in degrees as (ASHRAE Handbook Fundamentals, 2017):

$$H = 15(\text{AST} - 12) \tag{3.15}$$

H is zero at solar noon, positive in the afternoon, and negative in the morning.

$$H = 15(14.64 - 12) = 39.6^{o}$$

Solar declination δ, is the angle between the line joining the centers of the sun and the earth and its projection on the equatorial plane is given by following formula (ASHRAE Handbook Fundamentals, 2017):

$$\delta = 23.45 sin\left(360^{0}\,\frac{n+284}{365}\right) \tag{3.16}$$

$$\delta = 23.45 sin\left(360^{0}\,\frac{164+284}{365}\right)$$

$$\delta = 23.21^{0}$$

The altitude angle (β) is the angle in a vertical plane between the sun's rays and projection of sun's rays on the horizontal plane. Knowing the above parameters, the altitude angle β calculated as shown below (ASHRAE Handbook Fundamentals, 2017):

$$\sin\beta = \cos L\ \cos\delta\ \cos H + \sin L \sin\delta \tag{3.17}$$

$$\beta = \sin^{-1}(\cos L\ \cos\delta\ \cos H + \sin L \sin\delta)$$

$$\beta = \sin^{-1}(\cos 11.30\ \cos 23.21\ \cos 39.6 + \sin 11.30 \sin 23.21)$$

$$\beta = 50.50^{0}$$

The azimuth angle ϕ is the angle in the horizontal plane (i.e., horizon plane of the locality) measured from north to the horizontal projection of the sun's rays. The azimuth angle ϕ is uniquely determined by its sine and cosine, given in Equation 3.18 (ASHRAE Handbook Fundamentals, 2017):

$$\sin\phi = \frac{\sin H \cos\delta}{\cos\ \beta} \tag{3.18}$$

$$\sin \phi = \frac{\sin 39.6 \cos 23.21}{\cos\ 50.5}$$

$$\phi = 67.07^0$$

The position of the sun in the sky is specified by the zenith angle, angle between the sun's rays and the zenith, and azimuth angle, angle between the sun and reference direction.

The orientation of a receiving surface is best characterized by its tilt angle and its azimuth, shown in Figure 3.4. The tilt angle Σ is the angle between the surface and the horizontal plane. The surface azimuth ψ is defined as the displacement from south of the projection, on the horizontal plane, of the normal to the surface. Surface azimuths for common orientations are summarized in Table 3.4.

When the vehicle is moving its orientation changed randomly because of these all-azimuth angles are equal. At a time of 14:30(2:30 PM) from all orientation south west orientation ($\psi = 45^0$) sun of Semera has the maximum radiation load. When the bus is moving on the road orientation randomly changed, so to get maximum solar radiation load calculated in all direction.

Table 3.4. Surface orientations and azimuths measured from south (ASHRAE Handbook Fundamentals, 2017)

Orientation	**N**	**NE**	**E**	**SE**	**S**	**SW**	**W**	**NW**
Surface azimuth, ψ	180^o	-135^o	-90^o	-45^o	0	45^o	90^o	135^o

The surface-solar azimuth angle γ is defined as the angular difference between the solar azimuth ϕ and the surface azimuth ψ (ASHRAE Handbook Fundamentals, 2017).

$$\gamma = \phi - \psi \qquad 3.19$$

Finally, the angle between the line normal to the irradiated surface and the earth-sun line is called the angle of incidence θ. It is important in fenestration, load calculations, and solar technology because it affects the intensity of the direct component of solar radiation striking the surface and the surface's ability to absorb, transmit, or reflect the sun's rays. Its value is given by (ASHRAE Handbook Fundamentals, 2017):

$$\mathrm{Cos}\theta = \cos\beta \cos\gamma \sin\Sigma + \sin\beta\cos\Sigma \qquad 3.20$$

for vertical surfaces (Σ= 90°, cos Σ = 0, and sin Σ = 1) Equation 3.20 simplifies to

$$\cos \theta_{v} = \cos\beta \cos\gamma \qquad 3.21$$

For horizontal surfaces, Σ = 0°, sin Σ = 0, and cos Σ = 1, so Equation 3.20 leads to

$$\theta_{H} = 90 - \beta \qquad 3.22$$

Windshield glass is tilted backward 9° (Σ = 81°) from vertical surface and all the other glass surface of the bus is vertical, so for vertical surfaces (Σ = 90°) equation 3.21 is used.

the surface-solar azimuth angle for windshield glass is

$$\gamma = 67.07 - 45 = 22.07^{0}$$

To find the angle of incidence for windshield Equation 3.20 leads to

$$\mathrm{Cos}\theta = \cos 50.50 \cos 22.07 \sin 81 + \sin 50.50 \cos 81$$

$$\theta = 45.34^{0}$$

The angle of incidence for vertical surface glass

$$\cos \theta_{v} = \cos\beta \cos \gamma$$

$$\theta_{v} = \cos^{-1}(\cos\beta \cos\gamma) = \cos^{-1}(\cos 50.50 \cos 22.07)$$

$$\theta_{v} = 53.88°$$

Direct Radiant Load $\dot{Q}_{s,b}$

Direct normal irradiance E_{DN},

$$E_{DN} = \frac{A}{\exp\left(\frac{B}{\sin\beta}\right)}$$

From Table 3.3 the values of A = 1088 w/m^2 and B = 0.205.

$$E_{DN} = \frac{1088}{\exp\left(\frac{0.205}{\sin 50.50}\right)} = 834.16 \text{ W/m}^2$$

Surface direct irradiance E_D, of windshield glass ($\theta = 45.34^{0}$) is

$$E_D = 834.16 \text{W}/m^2 \cos 45.34 = 586.33 \text{ W}/m^2$$

Surface direct irradiance E_D, of vertical surface glass ($\theta_v = 53.88°$) is

$$E_D = 834.16 \text{W}/m^2 \cos 53.88 = 491.72 \text{ W}/m^2$$

From (ASHRAE Handbook Fundamentals, 1997), the value of SHGC is windshield and side glass is 0.77 and 0.78 respectively.

Heat gain from windshield glass

$$\dot{Q}_{s,b} = 0.77\ X\ 2.442m^2\ \mathrm{X}\ 586.33\ \mathrm{W}/m^2 = 1{,}102.50\ \mathrm{W}$$

Direct radiation load at the side glass of the bus

$$\dot{Q}_{s,b} = 0.78\ X\ 12.7736\ m^2\ \mathrm{X}\ 491.72\ \mathrm{W}/m^2 = 4{,}899.21\ \mathrm{W}$$

Direct radiation load at the back glass of the bus

$$\dot{Q}_{s,b} = 0.78\ X\ 0.985\ m^2\ \mathrm{X}\ 491.72\ \mathrm{W}/m^2 = 377.79\ \mathrm{W}$$

Then, Total heat gain from direct solar radiation

$$\dot{Q}_{s,b} = 1{,}102.50 + 4{,}899.21 + 377.79 = 6{,}379.50\ W$$

Diffuse Radiant Loads $\boldsymbol{\dot{Q}_{s,d}}$

Ratio Y of sky diffuse radiation on vertical surface to sky diffuse radiation on horizontal surface

$$Y = \max(0.45,\ 0.55 + 0.437\cos\theta + 0.313\ cos^2\ \theta$$

$$Y = \max(0.45,\ 0.55 + 0.437\cos(53.88) + 0.313\ cos^2(53.88) = 0.916$$

Diffuse irradiance E_{ds}, Vertical surfaces

$$E_{ds} = C\ Y\ E_{DN} \qquad \text{from Table 3.3, C = 0.134}$$

$$E_{ds} = 0.134\ X\ 0.916\ X\ 834.16\mathrm{W}/m^2 = 102.39\ \mathrm{W}/m^2$$

Diffuse irradiance E_{ds}, Surfaces other than vertical ($\Sigma = 81°$)

$$E_{ds} = 0.134\ X\ 834.16\mathrm{W}/m^2\ \left(\frac{1+\cos 81}{2}\right) = 64.63\ \mathrm{W}/m^2$$

Ground reflected irradiance E_{dg}, Vertical surfaces ($\Sigma = 90°$) is

$$E_{dg} = E_{DN}(C + \sin\beta)\rho_g\ \left(\frac{1-\cos\Sigma}{2}\right)$$

From Table 3.5, the values of reflectance of the ground ρ_g is 0.2

$$E_{dg} = 834.16\mathrm{W}/m^2\ (0.134 + \sin 50.5)0.2\ \left(\frac{1-\cos 90}{2}\right) = 75.54\ \mathrm{W}/m^2$$

Ground reflected irradiance E_{dg}, of windshield glass (Σ = 81°) is

$$E_{dg} = 834.16 \text{ W}/m^2 \ (0.134 + \sin 50.5)0.2 \left(\frac{1-\cos 81}{2}\right) = 63.72 \text{ W}/m^2$$

Table 3.5. Ground reflectance of foreground surface (ASHREA Handbook Fundamentals, 2017)

Foreground surface	**Reflectance**
Water (near normal incidences)	0.07
Coniferous forest (winter)	0.07
Asphalt, new	0.05
weathered	0.10
Bituminous and gravel roof	0.13
Dry bare ground	0.2
Weathered concrete	0.2 to 0.3
Green grass	0.26
Dry grassland	0.2 to 0.3
Desert sand	0.4
Light building surfaces	0.6

From (ASHRAE Handbook Fundamentals, 1997), the value of $\langle SHGC \rangle_D$ is windshield and side glass are 0.73 and 0.78 respectively.

Diffuse Radiant load at the windshield glasses of the bus

$$\dot{Q}_{s,d} = \langle SHGC \rangle_D \, A_g \, (E_{ds} + E_{dg})$$

$$\dot{Q}_{s,d} = 0.73 \, X \, 2.442 m^2 (64.63 \text{ W}/m^2 + 63.72 \text{ W}/m^2) = 228.80 \, W$$

Diffuse Radiant load at the side glasses of the bus (Σ = 90°) is

$$\dot{Q}_{s,d} = 0.78 \, X \, 12.7736 m^2 (102.39 \text{ W}/m^2 + 75.54 \text{ W}/m^2) = 1{,}772.79 \, W$$

Diffuse Radiant Load at the rear glass of the bus

$$\dot{Q}_{s,d} = 0.78 \, X \, 0.985 m^2 (102.39 \text{ W}/m^2 + 75.54 \text{ W}/m^2) = 136.70 \, W$$

Then, Total heat gain from reflected solar radiation

$$\dot{Q}_{s,d} = 228.80 + 1{,}772.79 + 136.70 = 2{,}138.29 \, W$$

Total Glass Solar Radiation Load is

$$\dot{Q}_{solar} = \dot{Q}_{s,b} + \dot{Q}_{s,d} = 6{,}379.50 + 2{,}138.29 = 8{,}517.79\,W$$

3.4.2 Heat gain through glass by conduction and convection

The heat transfer occurs at the glass surfaces not only by solar radiation, but also by conduction and convection, as calculated (ASHRAE Handbook Fundamentals, 1997; 2017):

$$\dot{Q}_{c,g} = U_g A_g (T_o - T_i) \qquad 3.23$$

Where Ag is area of glass and U_g is the overall heat transfer coefficient of the glass and, T_i and T_o are indoor and outdoor air temperature.

The U-factor for single glass is (ASHRAE Handbook Fundamentals, 1997; 2017):

$$U_g = \frac{1}{\frac{1}{h_o} + \frac{L}{k} + \frac{1}{h_i}} \qquad 3.24$$

Where h_o, h_i are outdoor and indoor glazing surface heat transfer coefficients, L is glass thickness, and k is thermal conductivity.

Outdoor surface heat transfer coefficient calculated by (ASHRAE Handbook Fundamentals, 1997):

$$h_o = 1.28 + 0.56V_w \qquad 3.25$$

Where V_w is average wind speed.

$$h_o = 1.28 + 0.56\ x\ 27.78 = 16.84\ \mathrm{W}/m^2k$$

For summer conditions inside surface heat transfer coefficient approximated to 8.29 W/m^2k (ASHRAE Handbook Fundamentals, 1997):

U_g for side window, door glass, back glass

$$U_g = \frac{1}{\frac{1}{16.84} + \frac{0.004}{0.8} + \frac{1}{8.29}}\ 5.405\ \mathrm{W}/m^2k$$

U_g for windshield glass

$$U_g = \frac{1}{\frac{1}{16.84} + \frac{0.006}{0.8} + \frac{1}{8.29}}\ 5.333\ \mathrm{W}/m^2k$$

Therefore, substituting the results in equation 3.20

For windshield glass:

$$\dot{Q}_{c,g} = 5.333\ x\ 2.442(44.5 - 24.5) = 260.45\ W$$

For side windows, door glass, and back glass:

$$\dot{Q}_{c,g} = 5.405\ x\ 13.7586(44.5 - 24.5) = 1{,}487.30\ W$$

Total heat gain by conduction through glass is

$$\dot{Q}_{c,g} = 260.45 + 1{,}487.30 = 1{,}747.76\ W$$

3.4.3 Heat gain through the bus body

The heat gains through the solid walls (side panels, roof, and floor); are each determined by the following equation:

$$\dot{Q}_{con} = UA(T_s - T_i) \qquad 3.26$$

Where A is area of opaque surface and U is the overall heat transfer coefficient of the surface element, T_s is surface temperature of the bus, and T_i is indoor temperature of the bus.

Overall heat transfer coefficient of the surface has different components consisting of the inside convection, conduction through the surface, and outside convection. It can be written in the form (ASHRAE Handbook Fundamentals, 2017):

$$U = \frac{1}{\frac{1}{h_o} + \frac{L}{k} + \frac{1}{k_a} + \frac{1}{h_i}} \qquad 3.27$$

Where h_o, h_i are outdoor and indoor convective heat transfer coefficient, L is wall thickness, k is thermal conductivity, and k_a is air gap.

Convective heat transfer coefficient as a function of vehicle speed estimated (Ingersoll, J., 1992)

$$h = 0.6 + 6.64\sqrt{V} \qquad 3.28$$

where V is the vehicle speed in m/s.

the ambient air velocity is considered equal to the vehicle velocity and cabin air velocity can be calculate by using the following formula (ASHRAE standard 55, 2017)

$$V_i = 50.49 - 4.4047(T_i) + 0.096425(T_i)^2$$

$$V_i = 50.49 - 4.4047(24.5) + 0.096425(24.5)^2 = 0.45\ m/s$$

Using the above formula inside and outside convection heat transfer can be calculated

$$h_i = 0.6 + 6.64\sqrt{0.45} = 5.054\ \mathrm{W}/m^2k$$

$$h_o = 0.6 + 6.64\sqrt{27.78} = 35.6\ \mathrm{W}/m^2k$$

Overall thermal conductivity of Car body

Left and hand side of body panel, front body panel and back body panel

$$U = \frac{1}{\frac{1}{35.6}+\frac{0.00225}{50.2}+\frac{0.04}{0.024}+\frac{1}{5.054}} = 0.528\ \mathrm{W}/m^2k$$

Roof panel

$$U = \frac{1}{\frac{1}{35.6}+\frac{0.00125}{50.2}+\frac{0.12}{0.024}+\frac{0.0025}{0.19}+\frac{1}{5.054}} = 0.191\ \mathrm{W}/m^2k$$

Floor

$$U = \frac{1}{\frac{1}{35.6}+\frac{0.002}{50.2}+\frac{1}{5.054}} = 4.425\ \mathrm{W}/m^2k$$

Akbari et al. (1996) studied surface temperature for given the solar reflectance and infrared emittance of a surface and developed the following equation that illustrate the importance of absorbance over surface temperature.

$$T_s = 310.04 + 82.49\alpha - 2.82\varepsilon - 54.33\alpha.\varepsilon + 21.72\alpha.\varepsilon^2 \qquad 3.29$$

Where α is solar absorbance of surface and ε is infrared emittance.

Starting from November 10, 2011 G.C the Federal Transportation Authority has color-coded long-distance buses according to their service level. Level One buses painted green stripe on top and white at the bottom, while level two blue stripes on top and white on the bottom and level three buses painted yellow stripe on the top and white on the bottom. Two third of bus painting color is white, so we calculate surface temperature using white surface solar reflectance and infrared emittance.

Solar absorbance calculates by:

$$\alpha = 1- \rho \qquad 3.30$$

where ρ is solar reflectance. So, from (ASHRAE Handbook Fundamentals, 1997) for standard white we get the value of reflectance 0.80 and emittance 0.90.

$$\alpha = 1\text{-}0.8 = 0.2$$

$$\varepsilon = 0.9$$

$$T_s = 310.04 + 82.49 \text{ x } 0.2 - 2.82 \text{ x } 0.9 - 54.330.2 \text{ x } 0.9 + 21.72 \text{ x } 0.2 \text{ x } 0.9^2$$

$$T_s = 317.73\text{k} = 44.58^oC$$

Heat gain from six surfaces of the bus

Left hand side of body panel

$$\dot{Q}_{con,L} = 0.528\ x\ 13.8412(44.58 - 24.5) = 146.75\ W$$

Right hand side of body panel

$$\dot{Q}_{con,R} = 0.528\ x\ 13.7966(44.58 - 24.5) = 146.27\ W$$

Front body panel

$$\dot{Q}_{con,F} = 0.528\ x\ 3.4613(44.58 - 24.5) = 36.70\ W$$

Rear body panel

$$\dot{Q}_{con,RR} = 0.528\ x\ 4.4243(44.58 - 24.5) = 46.91\ W$$

Roof panel

$$\dot{Q}_{con,RF} = 0.191\ x\ 21.6125(44.58 - 24.5) = 82.89\ W$$

Floor

$$\dot{Q}_{con,FL} = 4.425\ x\ 21.6125(44.58 - 24.5) = 1{,}879.26\ W$$

Total heat gain through opaque surface is

$$\dot{Q}_{con} = 146.75 + 146.27 + 36.70 + 46.91 + 82.89 + 1{,}879.26 = 2{,}338.78\ W$$

3.4.4 Heat gain from the Engine

Heat gain from the engine side of the vehicle was calculated from the following equation.

$$\dot{Q}_{engine} = UA_{eng}(T_{eng} - T_i) \qquad 3.31$$

Where U is overall heat transfer coefficient of the surface element in contact with the engine, A_{eng} surface area exposed to the engine temperature. Assume 15% of surface area of floor is subject to the engine temperature. T_{eng} is engine side air temperature. Assume the air temperature of the engine side 60°C. T_i is the indoor temperature of bus.

$$\dot{Q}_{engine} = 4.425\ x\ 3.1725(60 - 24.5) = 498.36\ W$$

3.4.5 Heat gain from the Exhaust

Heat gain from the Engine exhaust gas calculated by using following equation:

$$\dot{Q}_{exhaust} = UA_{exh}(T_{exhaust} - T_i) \qquad 3.32$$

Where U is overall heat transfer coefficient of the surface element in contact with the exhaust pipe, A_{exh} surface area exposed to the exhaust pipe temperature. Assume 5% of surface area of floor is subjected to the exhaust temperature. T_{exh} is exhaust pipe side air temperature. Assume the air temperature of the engine exhaust pipe side 60°C. T_i is the indoor temperature of bus.

$$\dot{Q}_{exhaust} = 4.425\ x\ 1.0575(60 - 24.5) = 166.12\ W$$

3.4.6 Heat from passengers

Heat transfer due to occupant consist both sensible as well as latent component.

$$\dot{Q}_{pass} = \dot{Q}_{pass,s} + \dot{Q}_{pass,l} \qquad 3.33$$

Where $\dot{Q}_{pass,s}$ is sensible heat gain due to passenger, $\dot{Q}_{pass,l}$ is latent heat gain due to passenger.

The sensible heat transfer rate due to occupant is given by:

$$\dot{Q}_{pass,s} = N(SHG_P)(CLF) \qquad 3.34$$

And the latent heat gain is:

$$\dot{Q}_{pass,l} = N(LHG_P) \qquad 3.35$$

Where N is number of people, SHG_P is sensible heat gain per person, LHG_P is latent heat gain per person, and CLF is cooling load factor for people.

The value sensible and latent heat gain per person estimated as 65 W and 30 W respectively. CLF = 1.0, if the cooling system is shut down during the night (ASHRAE Handbook Fundamentals, 1997).

Sensible heat gain from passenger

$$\dot{Q}_{pass,s} = \; 45 \; x \; 65 \; W \; x \; 1 = 2{,}925 \; W$$

Latent heat gain from passenger

$$\dot{Q}_{pass,l} = \; 45 \; x \; 30 \; W = 1{,}350 \; W$$

The total load due to passenger, by substitution in equation 3.33 is

$$\dot{Q}_{pass} = \; 2{,}925 + 1{,}350 = 4{,}275 \; W$$

3.4.7 Ventilation Load

Ventilation is intentional introduction of air from the outdoors into a bus internal compartment. The introduction of outdoor air for ventilation of conditioned spaces is necessary to dilute the odors given off by peoples and other internal air contaminants.

Heat transfer due to ventilation consist both sensible as well as latent component (ASHRAE Handbook Fundamentals, 1997; 2017):

$$\dot{Q}_v = \dot{Q}_{v,s} + \dot{Q}_{v,l} \qquad 3.36$$

Where $\dot{Q}_v$ is heat gain due to ventilation, is $\dot{Q}_{v,s}$ is sensible heat gain due to ventilation, and $\dot{Q}_{v,l}$ is latent heat gain due to ventilation.

The sensible heat transfer rate due to ventilation is given by (ASHRAE Handbook Fundamentals, 1997; 2017):

$$\dot{Q}_{v,s} = \dot{m}_v C_p (T_o - T_i) \qquad 3.37$$

Where $\dot{m}_v$ is mass flow rate of ventilated air, C_p is specific heat of moist ventilated air, For all practical purposes the humid specific heat of moist air, can be taken as 1.0216 kJ/kg dry air.K, T_o is outdoor dry bulb temperatures, and T_i is indoor dry bulb temperatures.

The latent heat transfer rate due to ventilation is given by (ASHRAE Handbook Fundamentals, 1997; 2017):

$$\dot{Q}_{v,l} = \dot{m}_v h_{fg}(\omega_o - \omega_i) \tag{3.38}$$

Where $\dot{m}_v$ is mass flow rate of ventilated air, h_{fg} the latent heat of vaporization of water, ω_o is the outdoor humidity ratio, and ω_i is indoor humidity ratio.

Mass flow rate of ventilated air is given by equation (ASHRAE Handbook Fundamentals, 1997; 2017):

$$\dot{m}_v = \frac{\dot{V}}{v_a} \tag{3.39}$$

Where $\dot{V}$ is ventilation rate and v_a is moist air specific volume.

It is recommended that ground mass transit applications use 3.5L/s of outdoor air per passenger for mass transit application (ASHRAE Handbook HVAC, 2019).

The ventilation rate is

$$\dot{V} = 45 persons\ x\ 3.5 L/s\ per\ person = 157.5\ L/s = 0.1575 \text{m}^3/\text{s}$$

From psychometric chart at elevation 633m (Dayton ASHRAE Online Psychrometric, 2020):
For inside conditions: 24.5^0 C (DBT) and 50% RH:

$$\omega_i = 0.01035\ \text{kg}_v/\text{kg}_a,\ h_i = 50.99\ \text{kJ/kg}$$

For outside conditions: 44.5^{o}C (DBT) and 21.815^{o}C (DPT):

$$\omega_o = 0.0178\ \text{kg}_v/\text{kg}_a,\ h_o = 90.72\ \text{kJ/kg},\ v_a = 0.998 \text{m}^3/\text{kg}$$

Mass flow rate of ventilated air is;

$$\dot{m}_v = \frac{\dot{V}}{v_a}$$

$$\dot{m}_v = \frac{0.1575}{0.998} == 0.1578 \text{kg/s}$$

Sensible heat transfer rate due to ventilation is

$$\dot{Q}_{v,s} = 0.1578 \text{kg/s x } 1.0216 \text{kJ/kg. k } (44.5 - 24.5) = 3{,}224.17 \text{W}$$

And latent heat transfer rate due to ventilation also calculated by

$$\dot{Q}_{v,l} = 0.1578 \text{kg/s x } 2501 \text{kJ/kg. } (0.0178 - 0.01035)\ \text{kgv/kga} = 2{,}940.2 \text{W}$$

Hence, Total heat gain due to ventilation by substituting equation 3.35.

$$\dot{Q}_v = \dot{Q}_{v,s} + \dot{Q}_{v,l} = 3{,}224.17 + 2{,}940.2 = 6{,}164.37\text{W}$$

3.4.8 Interior objects heat gain

Interior objects heat gain includes that produced by the evaporator fan motor, indoor lightings, driving electrical control devices, and electronics equipment's. For building air conditioning interior gain calculated by taking15% and 10% of room sensible and latent heat for interior object heat gain (Jordan and Prester, 1969). For our case let assume the total interior objects heat gain is 10% of sensible and latent heat.

$$\dot{Q}_{int} = 10\% \ (sensible\ and\ latent\ heat) = 0.1\ x\ 23{,}708.18 = 2{,}370.818\ W$$

3.4.9 Bus heating or air conditioning system load

The design cooling load (or heat gain) is the amount of heat energy to be removed from the bus by air conditioning equipment to maintain the bus at indoor design temperature when worst case outdoor design temperature is being experienced.

The total bus heating or air conditioning system load calculated using Equation 3.1

$$\dot{Q}_{solar} + \dot{Q}_{c,g} + \dot{Q}_{con} + \dot{Q}_{engine} + \dot{Q}_{exhaust} + \dot{Q}_{pass} + \dot{Q}_v + \dot{Q}_{int} + \dot{Q}_S = 0$$

$$\dot{Q}_S = -(8{,}517.79 + 1{,}747.76 + 2{,}338.78 + 498.36 + 166.12 + 4{,}275 + 6{,}164.37 + 2{,}370.82\ )W$$

$$\dot{Q}_S = -26{,}079\ W$$

Negative $\dot{Q}_S$ values represent cooling demands that must be satisfied by a cooling system. This means that that an equal amount of heat must be removed in order to keep the inside temperature at its specified value.

Total cooling loads required is 26,079 W, depending on outdoor weather conditions and geographic location.

Design supply airflow rate calculated from total cooling load as follow.

$$\dot{Q}_S = \dot{m}_v C_p \Delta T \qquad 3.40$$

Where $\dot{m}_v$ is mass flow rate, $C_p$is specific heat capacity of air, and ΔT is temperature difference between design supply and dry bulb temperature.

Cooling loads should be converted into volume flow rates but to do that first need to convert this to mass flow rate.

$$\dot{m}_v = \frac{\dot{Q}_S}{c_p \Delta T} \quad 3.41$$

$$\dot{m}_v = \frac{26.08\ kW}{(1.026\ kJ/kgk)(20k)} = 1.271\ kg/s$$

Now it can be converted into volume flow rate. To do that the specific volume or density of the air is needed. From psychometric chart at 24.5°C and assuming atmospheric pressure of 101.325kPa the value of specific volume is 0.85m^3/kg.

$$\dot{V} = \dot{m}_v\ x\ v_a = 1.271\ kg/s\ \ x\ 0.85\ m^3/kg$$

$$\dot{V} = 1.08\ m^3/s\ = 1080\ L/s$$

CHAPTER FOUR

DESIGN AND SIMULATION

4.1 Design and selection of air conditioning component

The calculated total cooling load provides information necessary to select all the components of HVAC system including packaged air-conditioning units, duct system, and diffusers.

4.1.1 Rooftop air-conditioning unit

Rooftop air-conditioning unit is constructed to include all the necessary component for air conditioning system within a single housing. The use of a rooftop bus air-conditioning system has been steadily growing in the emerging markets. Rooftop air conditioning units not only solve the problem of reducing the compartment interior space, but also improve the overall appearance. Besides that, more conducive to dissipate heat, and natural wind sucked into.

There are many rooftop air-conditioning unit's manufacturers in the world. Selection of appropriate Rooftop air conditioning unit for the designed bus from manufacturer catalogs is based on system and cooling load. Data obtained for selection purpose shown in Table 4.1:

Table 4.1. Specification of rooftop air conditioning units

Technical data	Requirements
Cooling capacity	26.08kW to 27kW
Evaporator air flow capacity	1080 L/s
Voltage	DC 24V
Compressor	Engine direct driven
Refrigerant	R 134a

Figure 4.1. Rooftop air conditioning unit (GUCHEN, 2015)

4.1.2 Ductwork design

For cost minimization and equal air distribution, one air diffuser was kept for every seat row on each side of the bus. Figure 4.2 and Figure 4.3 shows layout of passenger seat.

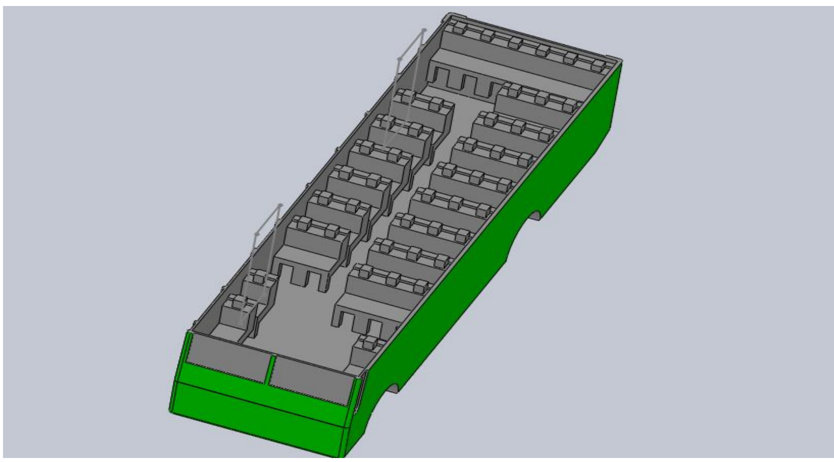

Figure 4.2. Passenger seat arrangement

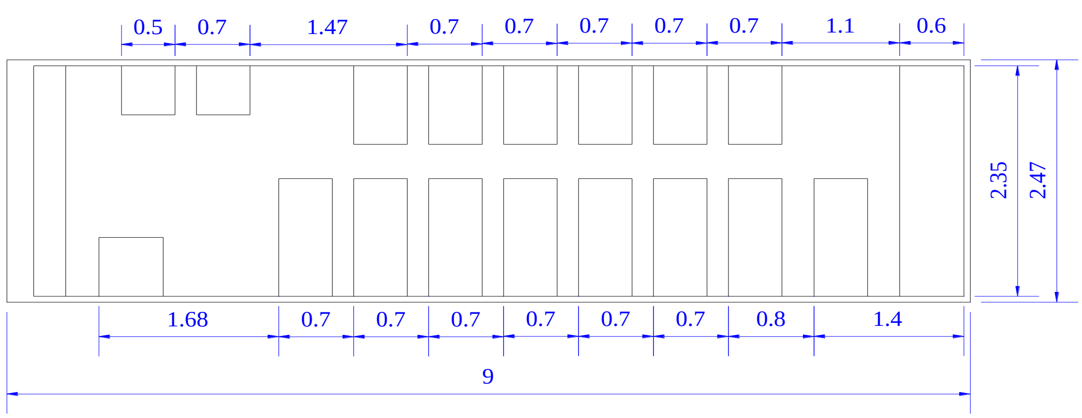

Figure 4.3. Passenger seat arrangement with dimensions

Ducts commonly used for carrying air are of round, square, or rectangular shape (Bhata, 2010). For this bus due to limitation of space rectangular shape duct was selected and also rectangular duct can fit above ceiling and they are much easier to install.

The most widely used method to size ducting is the equal friction method. The other methods are velocity reduction and static regain methods.

For conventional ductwork the equal friction method is recommended to be used. In this method, the average pressure or resistance to flow per unit length is kept at a constant (EBCS-11, 2014). The design procedure can be summarized as follows:

1. Choose a rate of pressure drop and keep this constant for the whole system.
2. Size ductwork using duct sizing chart or duct sizing programs if the volume flow rate of air is known. This will give the duct equivalent diameter.
3. Determine the equivalent size of rectangular duct if required by calculation, using tables or duct sizing programs and round.
4. Calculate the actual air velocity from:

$$v = \frac{Q}{A} \tag{4.1}$$

   Where v is Air velocity (m/s), Q is volume flow rate (m^3/s), and A is Cross sectional area of duct (m^2).

5. Determine pressure drop in straight duct taking pressure drop of about 1pa/m.
6. Determine fittings pressure loss as follows.

   - Determine the velocity pressure factors ($C_{\circ}$) for the fittings in each section of ductwork as given in the ASHRAE fittings database.
   - Determine the velocity pressure (p_v) using the following formula.

$$p_v = \frac{\rho v^2}{2} \tag{4.2}$$

   Where p_v is velocity pressure (Pa), ρ is Density of air, and v is Air velocity (m/s)

- Then pressure drop across the fitting (Δp) calculated using the following formula.

$$\Delta p = \mathrm{C}_{\circ}\frac{\rho v^2}{2} \qquad 4.3$$

7. Read pressure drop across filters, damper, grills, sound attenuators etc from catalogues.
8. Determine total pressure drop in each duct section consisting of pressure loss in straight duct and pressure loss for fittings and air distribution and control devices in that section.

$$\Delta p_j = \Delta p_{s.duct,j} + \sum_{i=1}^{m} C_i \frac{\rho v_i^2}{2} + \Delta p_{acess.,j} \qquad 4.4$$

9. Determine total pressure drop in the duct system by summing up the pressure drops in the sections.

$$\Delta p_{total} = \sum_{j=1}^{n} \Delta p_{j_i} \qquad 4.5$$

Using the above duct design procedure and duct sizer software (DesignTools DuctSizer Version 6.4) the supply duct is designed as show in Table 4.2.

For proper duct sizing, a pressure drop in a duct should be known for accurate design 1.0 Pa/m is recommended for pressure drop calculation for straight duct for accounting deviation from actual case (EBCS-11, 2014).

Table 4.2. Duct sizing sheet

DUCT SIZING TABLE													
Section	Fitting	ASHRAE fitting code	Length (m)	Flow Rate (L/s)	Pressure drop per meter (Pa/m)	Duct Size(mm)	Velocity (m/s)	Velocity Pressure (Pa)	Fittings pressure loss factor (C_o)	Pressure Loss		Section Total Pressure Loss (Pa)	Cumulative Pressure Loss (Pa)
										Fitting (Pa)	Straight Duct (Pa)		
Supply Duct Left Hand Side													
A	Duct		1.00	600.00	1.00	350X325	5.56	19.00			1.00	3.09	3.09
	Elbow, 90°	CR3-9							0.11	2.09			
Branch A	Duct		0.20	60.00	1.00	200X175	1.83	6.39			0.20	48.69	51.78
	Tee, 45°	SR5-13							7.59	48.49			
B	Duct		1.63	540.00	1.00	350X300	5.41	17.59			1.63	2.33	54.12
	Tee, 45°	SR5-13							0.04	0.70			
Branch B	Duct		0.20	60.00	1.00	200X175	1.83	6.39			0.20	48.69	102.81
	Tee, 45°								7.59	48.49			
C	Duct		0.70	480.00	1.00	350X275	5.26	17.09			0.70	1.38	104.19
	Tee, 45°	SR5-13							0.04	0.68			
Branch C	Duct		0.20	60.00	1.00	200X175	1.83	6.39			0.20	48.69	152.88
	Tee, 45°								7.59	48.49			
D	Duct		0.70	420.00	1.00	350X250	5.09	15.96			0.70	1.34	154.22
	Tee, 45°	SR5-13							0.04	0.64			
Branch D	Duct		0.20	60.00	1.00	200X175	1.83	6.39			0.20	20.01	174.23
	Tee, 45°								3.10	19.81			
E	Duct		0.70	360.00	1.00	300X250	4.90	15.80			0.70	1.33	175.56
	Tee, 45°	SR5-13							0.04	0.63			
Branch E	Duct		0.20	60.00	1.00	200X175	1.83	6.39			0.20	10.74	186.30
	Tee, 45°								1.65	10.54			
F	Duct		0.70	300.00	1.00	300X225	4.68	13.62			0.70	1.24	187.55
	Tee, 45°	SR5-13							0.04	0.54			
Branch F	Duct		0.20	60.00	1.00	200X175	1.83	6.39			0.20	10.74	198.29
	Tee, 45°								1.65	10.54			
G	Duct		0.70	240.00	1.00	275X200	4.43	13.15			0.70	1.23	199.52
	Tee, 45°	SR5-13							0.04	0.53			
Branch G	Duct		0.20	60.00	1.00	200X175	1.83	6.39			0.20	10.74	210.26
	Tee, 45°								1.65	10.54			
H	Duct		0.70	180.00	1.00	250X175	4.12	11.75			0.70	1.17	211.43
	Tee, 45°	SR5-13							0.04	0.47			
Branch H	Duct		0.20	60.00	1.00	200X175	1.83	6.39			0.20	8.38	219.81
	Tee, 45°								1.28	8.18			
I	Duct		0.70	120.00	1.00	225X175	3.26	8.80			0.70	1.05	220.86
	Tee, 45°	SR5-13							0.04	0.35			
Branch I	Duct		0.20	60.00	1.00	200X175	1.83	6.39			0.20	6.78	227.64
	Tee, 45°								1.03	6.58			
J	Duct		1.05	60.00	1.00	200X175	1.83	6.39			1.05	2.01	229.65
	Tee, 45°	SR5-13							0.04	0.26			
	Elbow, 90°								0.11	0.70			

Supply Duct Right Hand Side													
A	Duct		1.71	480.00	1.00	350X275	5.26	17.09			1.71	3.59	3.59
	Elbow, 90°	CR3-9							0.11	1.88			
Branch A	Duct		0.20	60.00	1.00	200X175	1.83	6.39			0.20	48.69	52.28
	Tee, 45°								7.59	48.49			
B	Duct		1.83	420.00	1.00	350X250	5.09	15.96			1.83	2.47	54.75
	Tee, 45°	SR5-13							0.04	0.64			
Branch B	Duct		0.20	60.00	1.00	200X175	1.83	6.39			0.20	48.69	103.44
	Tee, 45°								7.59	48.49			
C	Duct		0.70	360.00	1.00	300X250	4.90	15.80			0.70	1.33	104.78
	Tee, 45°	SR5-13							0.04	0.63			
Branch C	Duct		0.20	60.00	1.00	200X175	1.83	6.39			0.20	10.74	115.52
	Tee, 45°								1.65	10.54			
D	Duct		0.70	300.00	1.00	300X225	4.68	13.62			0.70	1.24	116.76
	Tee, 45°	SR5-13							0.04	0.54			
Branch D	Duct		0.20	60.00	1.00	200X175	1.83	6.39			0.20	10.74	127.50
	Tee, 45°								1.65	10.54			
E	Duct		0.70	240.00	1.00	275X200	4.43	13.15			0.70	1.23	128.73
	Tee, 45°	SR5-13							0.04	0.53			
Branch E	Duct		0.20	60.00	1.00	200X175	1.83	6.39			0.20	10.74	139.47
	Tee, 45°								1.65	10.54			
F	Duct		0.70	180.00	1.00	250X175	4.12	11.75			0.70	1.17	140.64
	Tee, 45°	SR5-13							0.04	0.47			
Branch F	Duct		0.20	60.00	1.00	200X175	1.83	6.39			0.20	8.38	149.02
	Tee, 45°								1.28	8.18			
G	Duct		0.70	120.00	1.00	225X175	3.26	8.80			0.70	1.05	150.07
	Tee, 45°	SR5-13							0.04	0.35			
Branch G	Duct		0.20	60.00	1.00	200X175	1.83	6.39			0.20	6.78	156.85
	Tee, 45°								1.03	6.58			
H	Duct		1.65	60.00	1.00	200X175	1.83	6.39			1.65	2.61	159.46
	Tee, 45°	SR5-13							0.04	0.26			
	Elbow, 90°	CR3-9							0.11	0.70			
Return Duct													
A	Duct		2.35	1,080.00	1.00	450X400	5.83	23.97			2.35	2.35	2.35
Branch A	Duct		0.10	540.00	1.00	400X300	3.94	9.91			0.10	14.17	16.52
	Tee, 45°								1.42	14.07			
B	Duct		3.50	540.00	1.00	400X300	3.94	9.91			3.50	18.66	35.17
	Tee, 45°	SR5-13							1.42	14.07			
	Elbow, 90°	CR3-9							0.11	1.09			

Figure 4.4 is a sketch of the layout of an air distribution system inside bus compartment. There are 8 inlet diffusers on right hand side and 10 on the left hand side of bus compartment. And there are two return grills as shown on Figure 4.4.

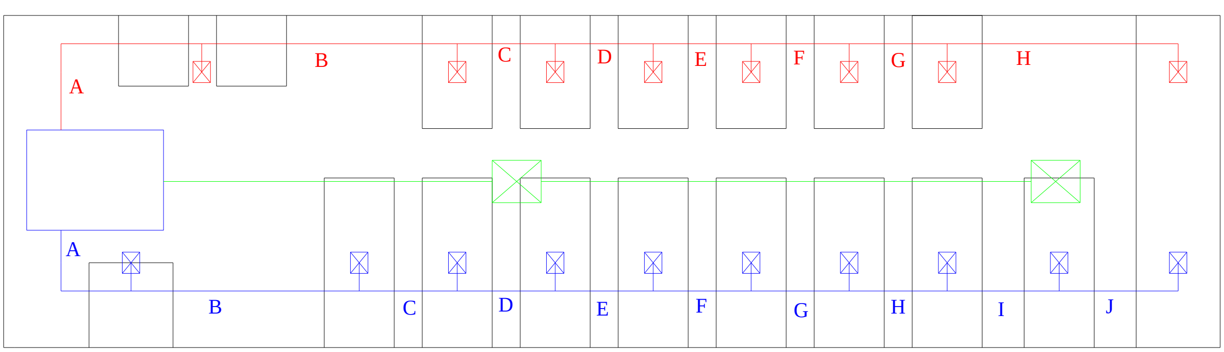

Right hand side supply line   Left hand side supply line   Return line

Figure 4.4. Schematic duct layout

4.1.3 Diffusers selection

A ventilation diffuser disperses pressurized air exiting air conditioning ductwork and provide a decorative finish over the grill box hole holding the ductwork in place. Without an air diffuser, the air exiting the HVAC system would travel in a straight direction. This causes a concentration of conditioned air in one section of the space while the rest of the space remains unconditioned. The direction that a vent diffuser sends flowing air depends on the direction of the diffuser fins.

Supply diffuser selection

For supply diffusers, the following points are considered on selection process. Selection should be made from manufacturers catalogues.

For equal air distribution there are 18 inlet diffusers

Flow rate at branch side = 1080/18 = 60 L/s= 0.06m^3/s

Flow area at diffuser is determined as

$$A_{diffuser} = \frac{Q_s}{V_s} \qquad 4.6$$

Where Q_s is flow rate of supply air and V_s is velocity of supply air

$$A_{diffuser} = \frac{0.06\ m^3/s}{1.8293\ m/s} = 0.0328\ m^2$$

Selection should be made from manufacturers catalogs linear slot diffuser with flow rate 0.06m^3/s and diffuser area of 0.0328 m^2.

Slot diffusers can be installed individually in set lengths or in a continuous line. They can also be installed in any type of ceiling application. The air pattern control is adjustable from the diffuser face and is achieved by means of an adjustable pattern control with each slot, enabling a full 180^o air pattern adjustment.

Air return grill selection

A return air grill connects to ductwork that allows air to return to any cooling system. Every cooling system will have air being pushed though into rooms and spaces through a system of ducts. This increases the air pressure in the conditioned area and at some time will act to even prevent any further air from entering unless a circulating system is set up to relieve the pressure. This is done normally through return ducts which allow the air to be recirculated or completely vented to the outside in certain cases. A return air grill will cover such ducts, and can also act to regulate the flow of air.

There will be two pieces of return grill on the ceiling

Flow rate at each return grill = 1080/2 = 540 L/s= 0.54 m^3/s

Flow area at return grill is determined as

$$A_{grill} = \frac{Q_s}{V_s}$$

Where Q_s is flow rate of supply air and V_s is velocity of supply air

$$A_{grill} = \frac{0.54\ m^3/s}{3.942\ m/s} = 0.137\ m^2$$

Selection should be made from manufacturer catalogs air return grill with flow rate 0.54 m^3/s and diffuser area of 0.137 m^2.

4.2 CFD modeling and simulation

In this thesis a multi-purpose computational fluid dynamic software ANSYS Fluent was employed to simulate air flow conditions inside the bus passenger compartment and examine the variation of concentrations of temperature at several locations inside the bus compartment. The main steps of the simulation are briefly described below.

4.2.1 Geometric modeling

A three-dimensional model of the long-distance bus was developed by using SolidWorks 2013 and ANSYS Design Modeler with having the dimensions of 9m in length, 2.47m in width and 2.39 in height. As seen from the Figure 4.5 the bus has total of 44 passenger seats. To provide conditioned air to bus compartment there are 18 inlet diffusers located on the ceiling and two outlets located, one in the middle and the other at the rear side of ceiling. The arrangement of ducts is modelled for overhead air distribution system which are placed in the ceiling of the bus. For every seat on each side of the bus there is one inlet on the roof.

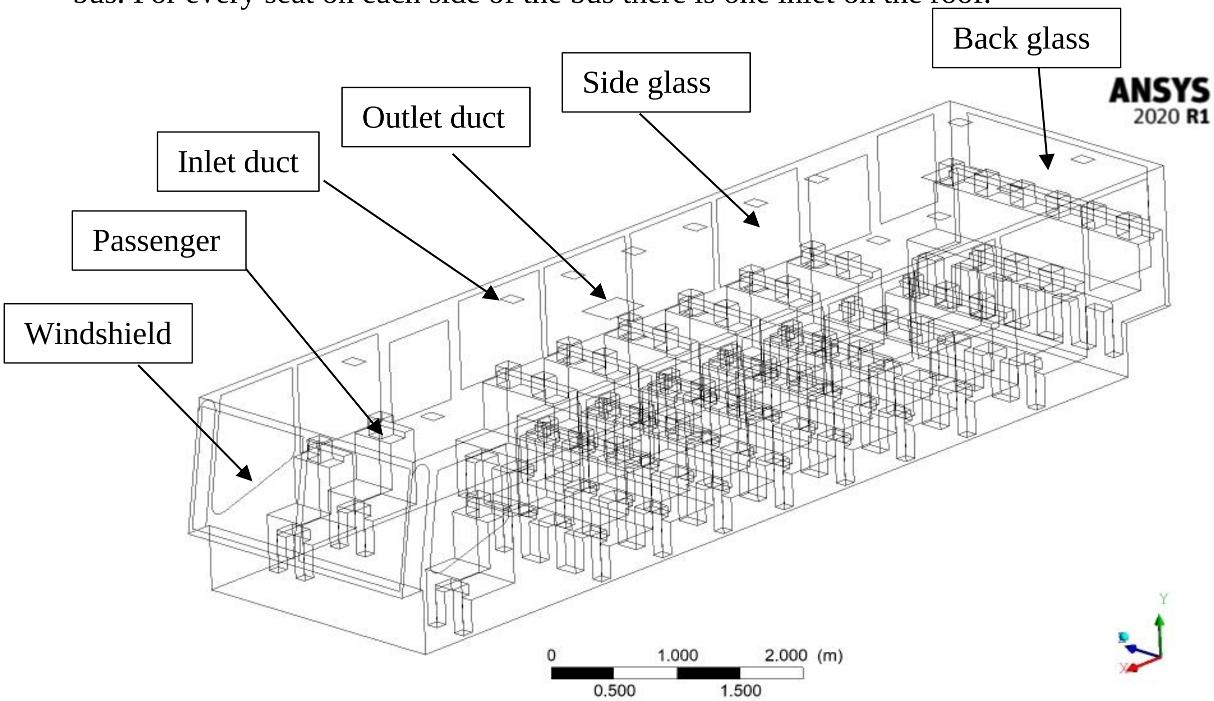

Figure 4.5. Geometry of the bus passenger compartment

4.2.2 Mesh generation

To be able to simulate air flow in the bus, mesh generation was needed. The mesh divides the bus into small elements so the ANSYS software can calculate the flow at each element of the mesh. The smaller the mesh base size, the more accurate the simulation will be. In this study, the volume mesh is created using Fluent Meshing which allows the geometry for a higher mesh quality and the creation of polyhedral meshes which reduces the total number of cells and the amount of calculation time. The model was meshed using polyhedral elements, as shown in Figure 4.6. The result of curvature and proximity sizing controls applied to the inlets and outlets can be observed from the Figure 4.6 and Figure 4.7. This is to ensure that the CFD analysis results are more accurate.

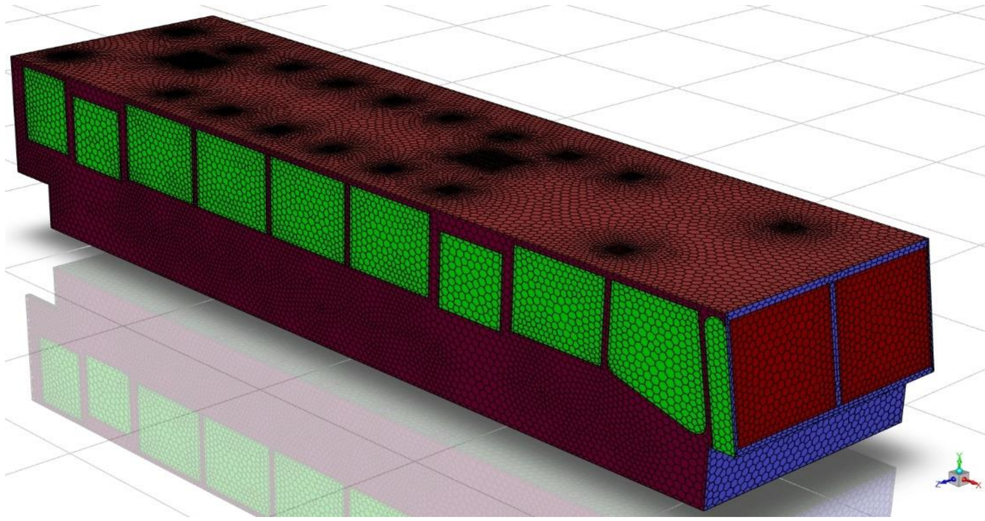

Figure 4.6. Meshed CFD model.

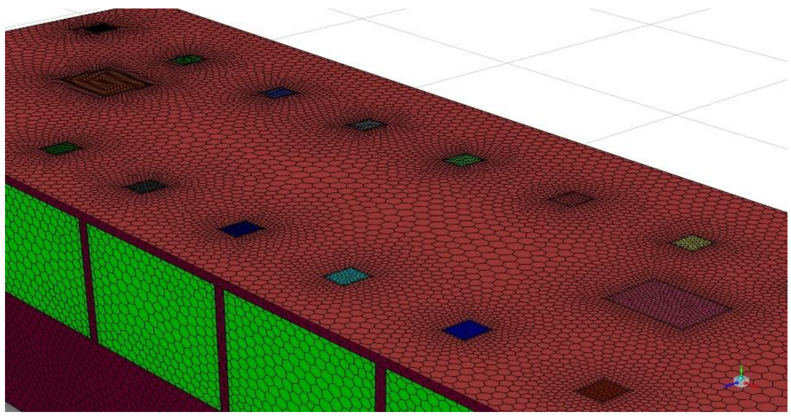

Figure 4.7. Mesh structure in the inlet and outlet

4.2.3 Boundary condition

The CFD analysis on the bus passengers' compartment was performed in order to investigated the condition of the air velocity and temperature distributions in the compartment under a given set of conditions. To do this, certain boundary condition was prescribed on the passenger compartment model involving three parameters namely air velocity at the air conditioning inlet vents, air temperature, heat gain through the compartment wall.

The air flow velocity at the supply diffusers were prescribed at 1.8293 m/s. The exterior temperature of the numerical simulation was set to as a constant value of 44.5 °C. Heat Transfer by radiation is considered from all bus cabin windows. The emissivity for interior surfaces equals 0.95 (Soliman, 2020) and for glass equals 0.88 (Mezrhab and Bouzidi, 2006). Also, all windows and the bus door were assumed to be closed and there were 44 passengers inside the bus compartment. Assume that the temperature of passenger surface was constant and it was set to 34^{o}C (k = 0.21 W/m.k, ρ =1,000 kg/m^3 , C_p = 3,770 J/kg.k) (Rugh and Bharathan, 2005). Details on the boundary conditions that are used in the CFD simulations are shown in Table 4.3 below.

Table 4.3. Boundary conditions

Localization	**Parameters**	**Value**
air supply	Inlet velocity [m/s]	1.8293
	Inlet temperature [°C]	20
	Number of inlets	18
	Number of outlets	2
Windshield glass	Direct irradiance [W/m^2]	586.33
	Diffuse irradiance [W/m^2]	128.35
	Heat transfer coefficient [W/m^2. k]	16.84
Sides and back glass	Direct irradiance [W/m^2]	491.72
	Diffuse irradiance [W/m^2]	177.93
	Heat transfer coefficient [W/m^2. k]	16.84
Right & left hand side body panel	Heat transfer coefficient [W/m^2. k]	35.6
Front and back body panel	Heat transfer coefficient [W/m^2. k]	35.6
Roof	Heat transfer coefficient [W/m^2. k]	35.6
Floor	Heat transfer coefficient [W/m^2. k]	35.6
Passengers	Number of passengers + Driver	45
	Passenger body surface temperature [°C]	34

4.2.4 Flow analysis

The CFD simulation was carried out using ANSYS Fluent 2020 R1 software. The advantages of using this software is advanced solver technology, accurate CFD results, efficient and flexible workflow, solve complex models, turbulence modeling (ANSYS, 2020).

Each turbulence model has its own advantages and disadvantages. There are no universal turbulence models for air flow simulation. The selection of a suitable model depends mainly on accuracy needed and computing time afforded (Zhai et al., 2007).

In this study, the SST $k - \omega$ turbulence model is used to capture thermal effects near the walls with good accuracy for the velocity field as well (ANSYS Fluent 12.0, 2009; Zhai et al., 2007).

The CFD analysis was carried out at a steady-state condition using a pressure-based coupled algorithm. The convergence criteria were set as 10^{-6} for energy and 10^{-3} for all the other parameters (ANSYS Fluent 12.0, 2009). Table 4.4 shows the boundary conditions and the numerical parameters used for 3-D CFD simulation.

Table 4.4. Main simulation settings on Fluent

Solver Type	Pressure-based			
Time	Steady			
Model	Viscous SST k - ω			
Radiation Model	Discrete Ordinates (DO)			
Materials	Fluid	Air	Density	1.225 kg/m^3
			Specific heat capacity	1006.43 J/kg.k
			Thermal conductivity	0.0242 W/m.k
	Solid	Glass	Density	2500 kg/m^3
			Specific heat capacity	871 J/kg.k
			Thermal conductivity	0.8 W/m.k
		Steel	Density	7833 kg/m^3
			Specific heat capacity	465 J/kg.k
			Thermal conductivity	54 W/m.k
		Human Body	Density	1000 kg/m^3
			Specific heat capacity	3770 J/kg.k
			Thermal conductivity	0.21 W/m.k
Cell zone conditions	Fluid			
Boundary Conditions	Inlet		Velocity	1.8293 m/s
			Hydraulic diameter	0.18667 m
			Back flow turbulent intensity	5.00%
	Outlet		Gauge total Pressure	0 kPa
			Back flow turbulent intensity	5.00%
	Windshield glass		Material	Glass

		Heat transfer coefficient	16.84W/m^2. k
		Free stream temperature	44.5^{o}C
		Direct irradiation	586.33 W/m^2
		Diffuse irradiation	128.35 W/m^2
	Sides and back glass	Material	Glass
		Heat transfer coefficient	16.84 W/m^2. k
		Free stream temperature	44.5^{o}C
		Direct irradiation	491.72 W/m^2
		Diffuse irradiation	177.93 W/m^2
	Front, sides and back body	Material	Steel
		Heat transfer coefficient	35.6 W/m^2. k
		Free stream temperature	44.5^{o}C
	Roof	Material	Steel
		Heat transfer coefficient	35.6 W/m^2. k
		Free stream temperature	44.5^{o}C
	Floor	Material	Steel
		Heat transfer coefficient	35.6 W/m^2. k
		Free stream temperature	44.5^{o}C
	Surface area exposed to the Engine Temperature (15% of floor)	Material	Steel
		Heat transfer coefficient	35.6 W/m^2. k
		Free stream temperature	60^{o}C
	Surface area exposed to the Exhaust pipe Temperature (5% of floor)	Material	Steel
		Heat transfer coefficient	35.6 W/m^2. k
		Free stream temperature	60^{o}C
	Passenger	Material	Human body
		Temperature	34^{o}C
Solution Methods	Scheme	SIMPLE	
Convergence Criteria		10^{-6} for energy and 10^{-3} for all the other	

4.2.5 Grid independence test

A CFD solution can never be trusted unless we check whether the result depends on the grid or not. The output result of a coarser mesh and finer mesh may not be the same. Therefore, a number of simulations were performed using computational grids with varying cell sizes. By comparing the predicated temperature and airflows patterns produced by simulations with different cell sizes, grid independence was established.

In this study, three different mesh structures are generated having different number of elements as shown in Table 4.5. The temperature was chosen as a reference parameter to determine the independent mesh convergence solution.

As seen in Figure 4.8 twelve lines inside bus compartment are taken to compare the temperature for grid independency test. Grid independence test results are shown in Figure 4.9.

Table 4.5. Parameters used in the grid independence test

	Mesh 1	**Mesh 2**	**Mesh 3**
Number of elements	321,223	333,913	382,402

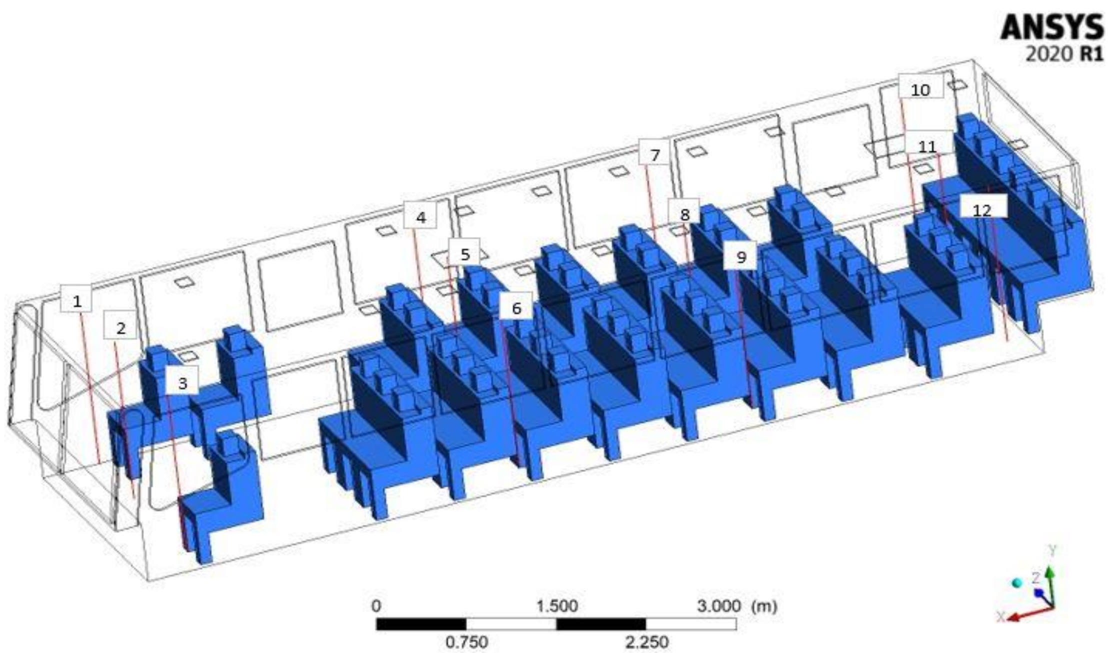

Figure 4.8. Temperature measuring line for grid independence test

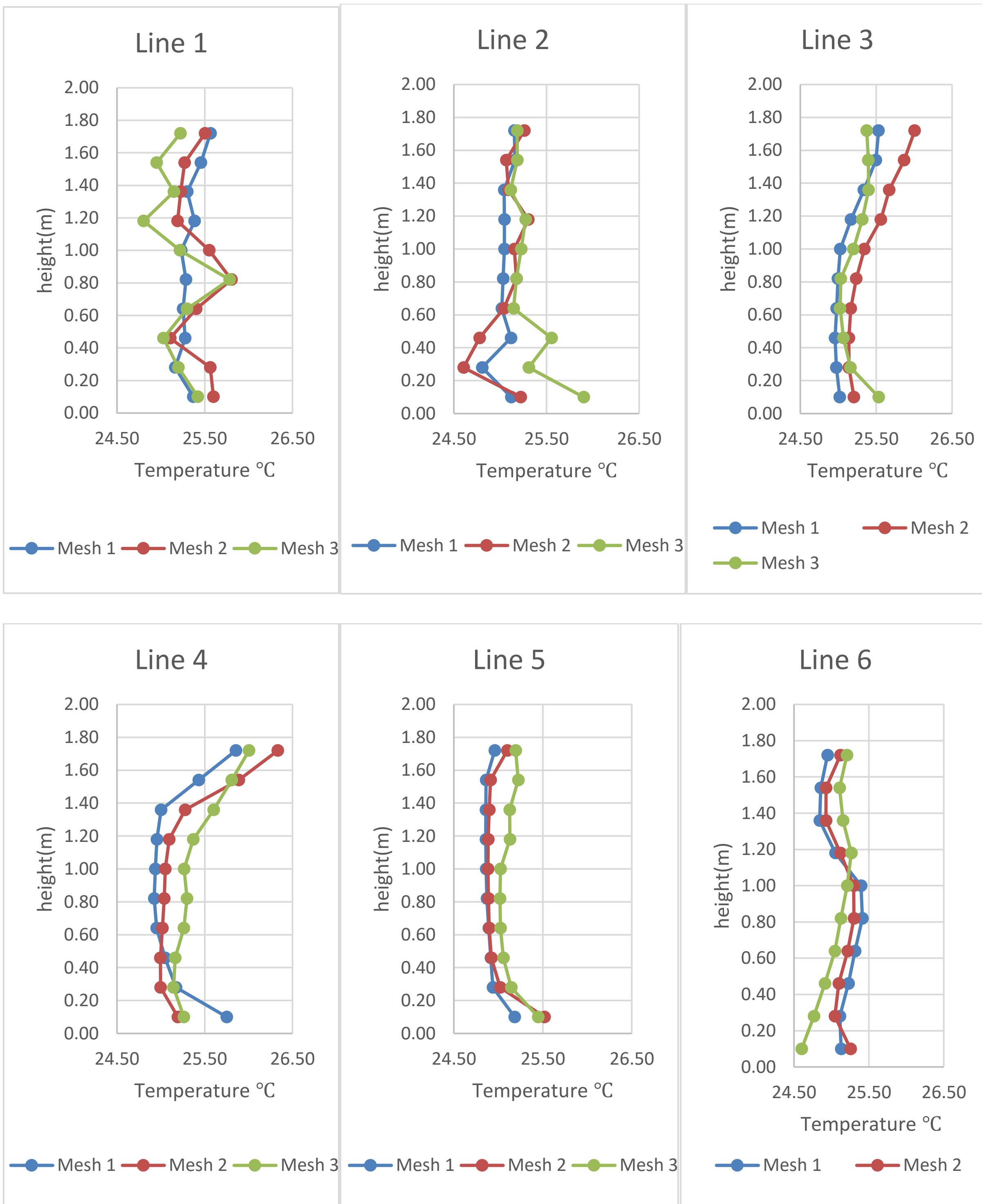

Line 1
Line 2
Line 3
Line 4
Line 5
Line 6
height(m)
Temperature ℃
2.00
1.80
1.60
1.40
1.20
1.00
0.80
0.60
0.40
0.20
0.00
24.50
25.50
26.50
Mesh 1
Mesh 2
Mesh 3

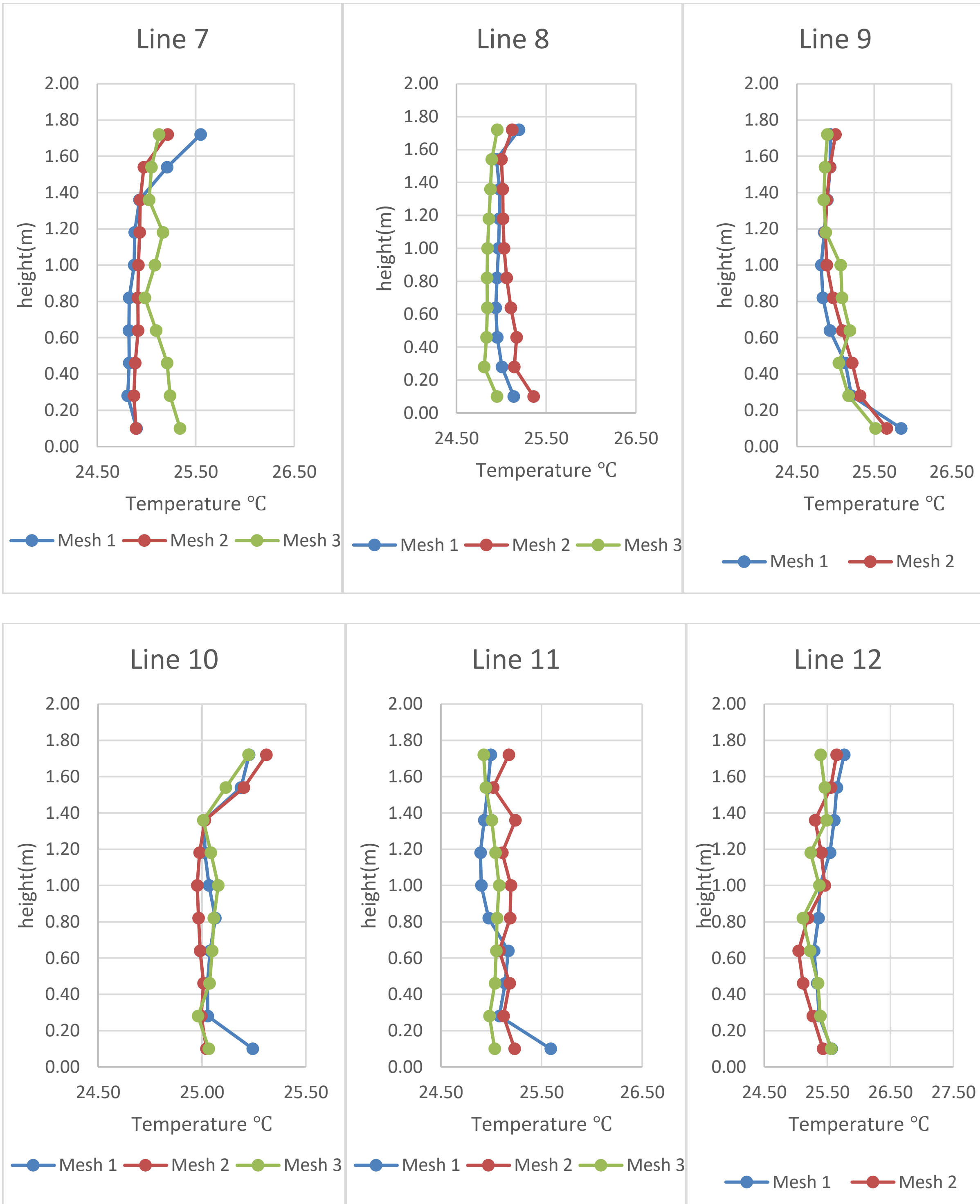

Figure 4.9. Temperature reading in the grid independence test

From the Figure 4.9 the results obtained from the three types of meshes do not demonstrate a significant difference from each other. The solver can simulate a relatively faster using coarse mesh, Mesh 1 was chosen for the rest of this CFD model.

As shown in Figure 4.10, the simulation converged with 5,000 iterations. A solution is said to be converged in a steady state simulation when the line of the convergence plot stops varying and the slope becomes zero. The data processing time for each simulation was around 6 hours using 64-bit processors (Intel (R) core i7-7600U CPU @ 2.8GHz, SSD Hard disk, installed RAM 16GB).

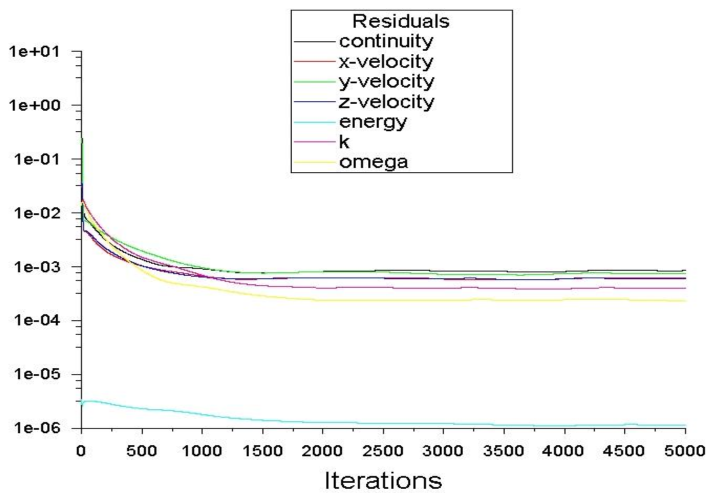

Figure 4.10. Convergence history of the residuals

CHAPTER FIVE

RESULTS AND DISCUSSION

The cooling load analysis for vehicle applications different from stationary, building based systems because vehicle orientation and occupant density changes regularly. In this thesis, the method used in calculating the cooling load is the heat balance method.

Total cooling loads of 26,079 W is calculated, depending on outdoor weather conditions and geographic location. The typical distribution of the different heat loads during the hottest month of the year at 11^0 30' North latitude and 41^0 12' East longitude is shown in Figure 5.1.

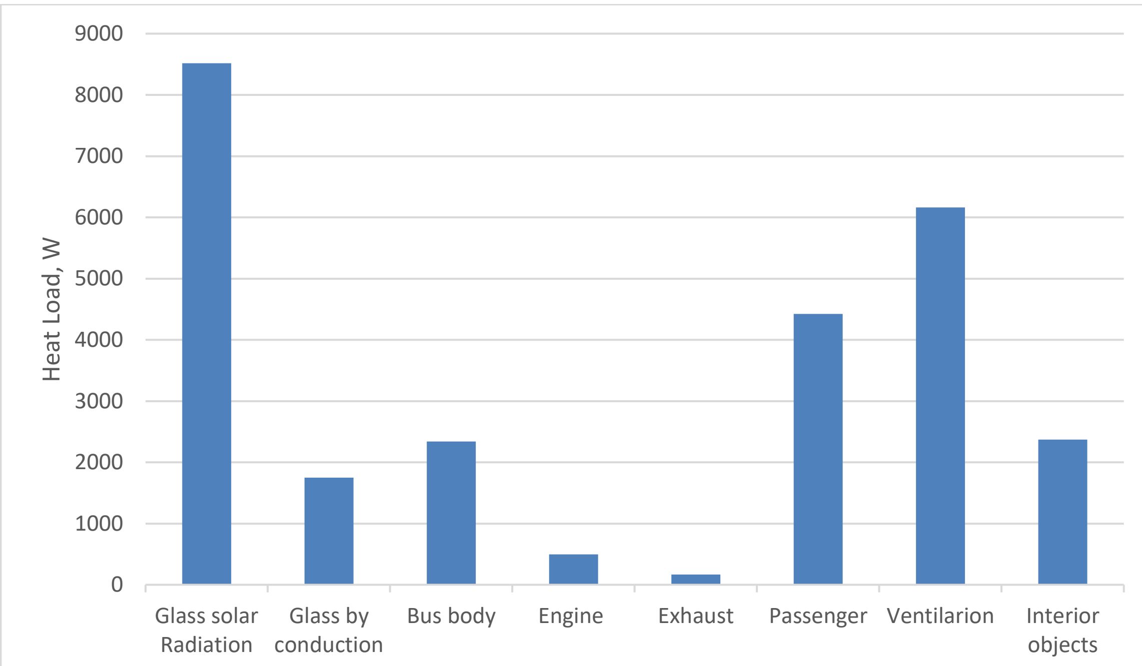

Figure 5.1. Typical main heat fluxes in bus

5.1 Analysis of indoor air velocity and temperature

In this section, the simulation results of air circulation and temperature distribution inside passenger compartment shown using different plots and figures as well with values.

It is important for air conditioning system to ensure the rationality of inlet air distribution because it is closely related to the effect of adjusting indoor temperature, human body comfort.

In this study, the air and temperature distributions are presented based on the CFD simulation for supply air inlet temperature 20°C and inlet velocity of 1.8293 m/s.

5.1.1 Distribution of air temperature

The simulation shows the design angle of the inlet diffuser performs a great integration with supplied air blowing towards area between the passengers and seats providing a relatively homogeneous distribution to passengers (Figure 5.2).

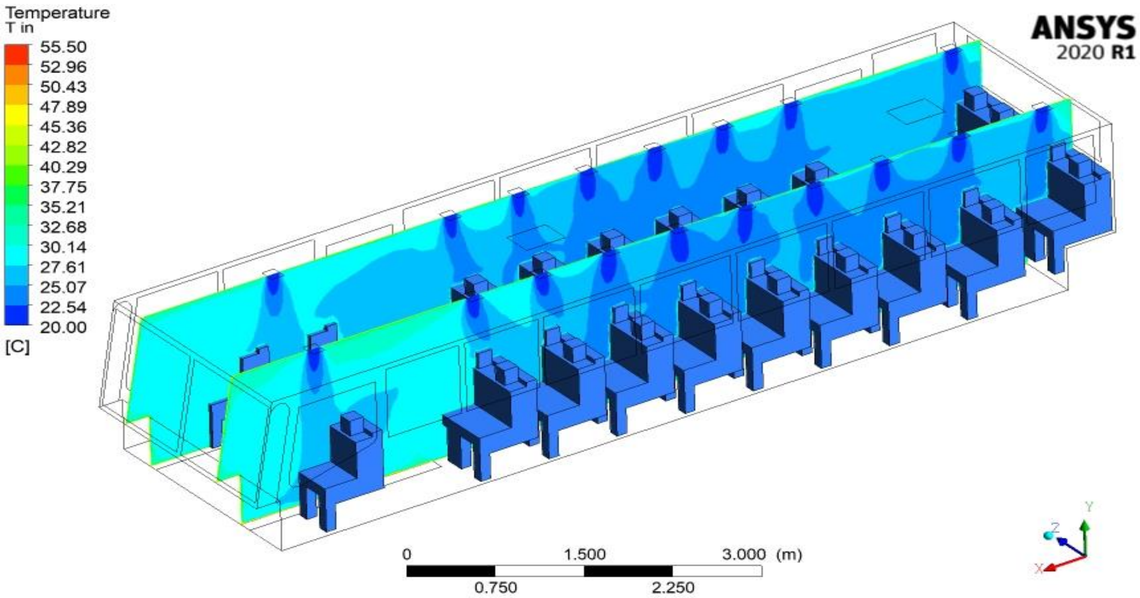

Figure 5.2. Temperature contour plot at inlets duct on X-Y plane.

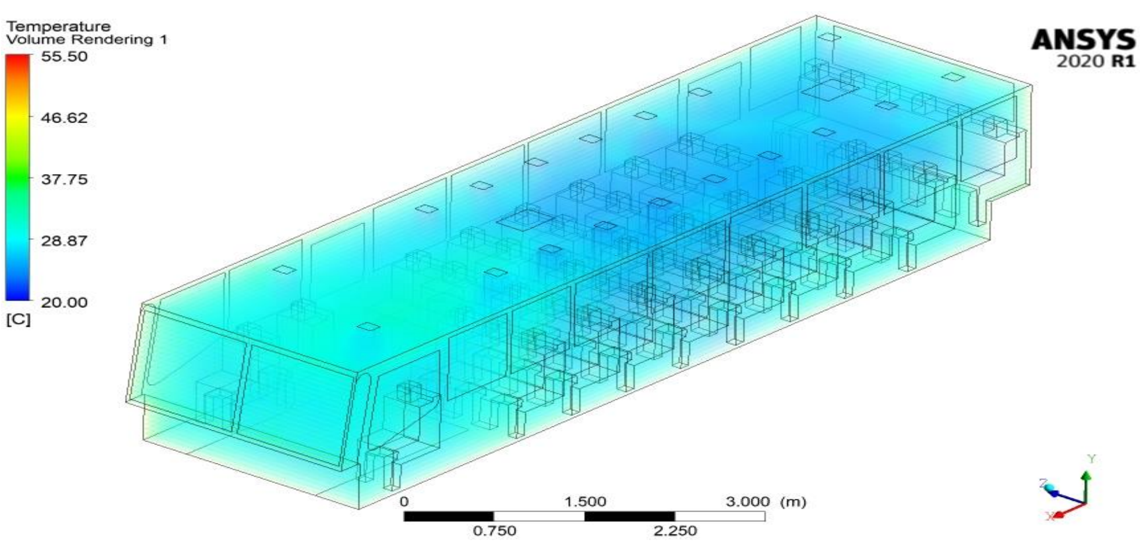

Figure 5.3. Temperature distribution in bus compartment.

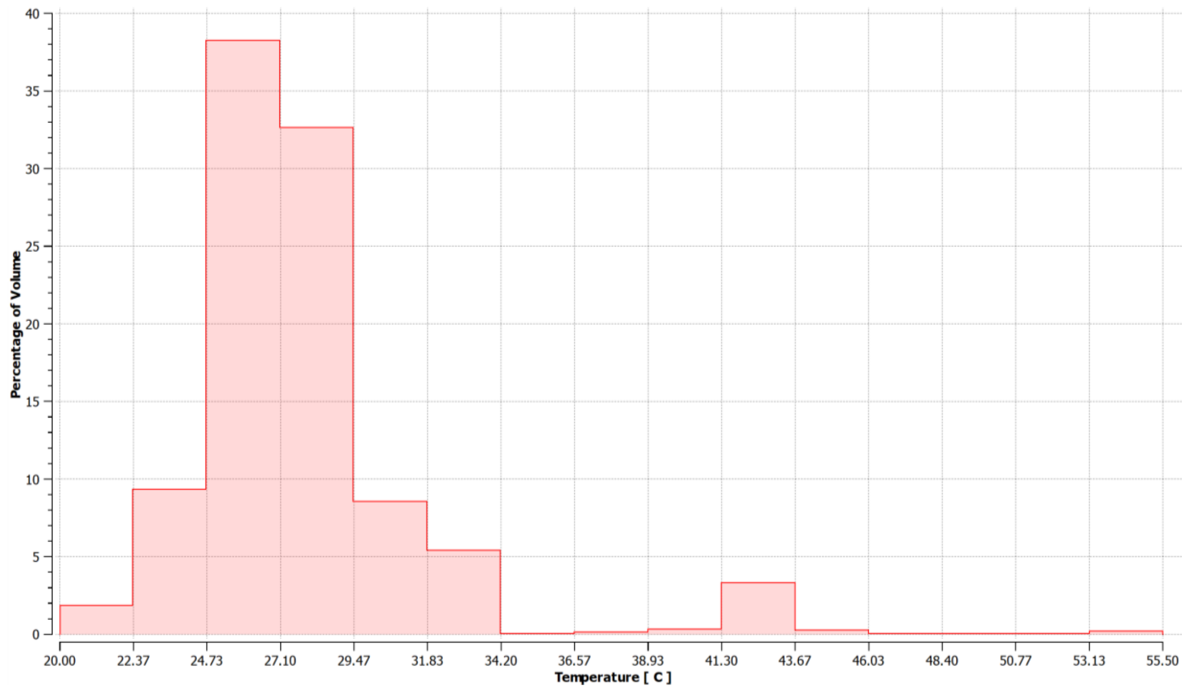

Figure 5.4. Graph of temperature distribution in bus compartment.

Figure 5.3 and Figure 5.4 shows the temperature distribution inside of bus compartment. The temperature of air flow through duct is 20 °C and body surface having temperature of 34 °C.

To measure temperatures of air in the bus compartment three horizontal planes were used. Location of three planes: A in the axis of heads, B in the axis of knees and C in the axis of ankles of sitting passenger (Figure 5.5). They were located 0.1m, 0.6m, and 1.1m above floor level.

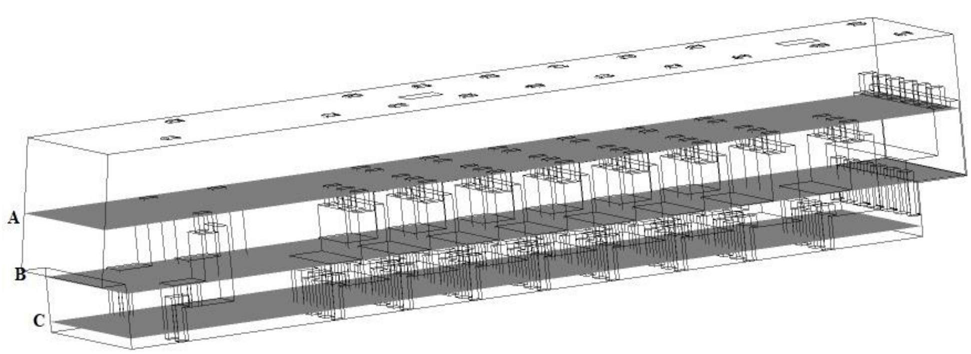

Figure 5.5. Temperature measuring planes.

Figure 5.6 to Figure 5.8 shows the results of the bus compartment air temperature distribution at head, knee, and ankle level.

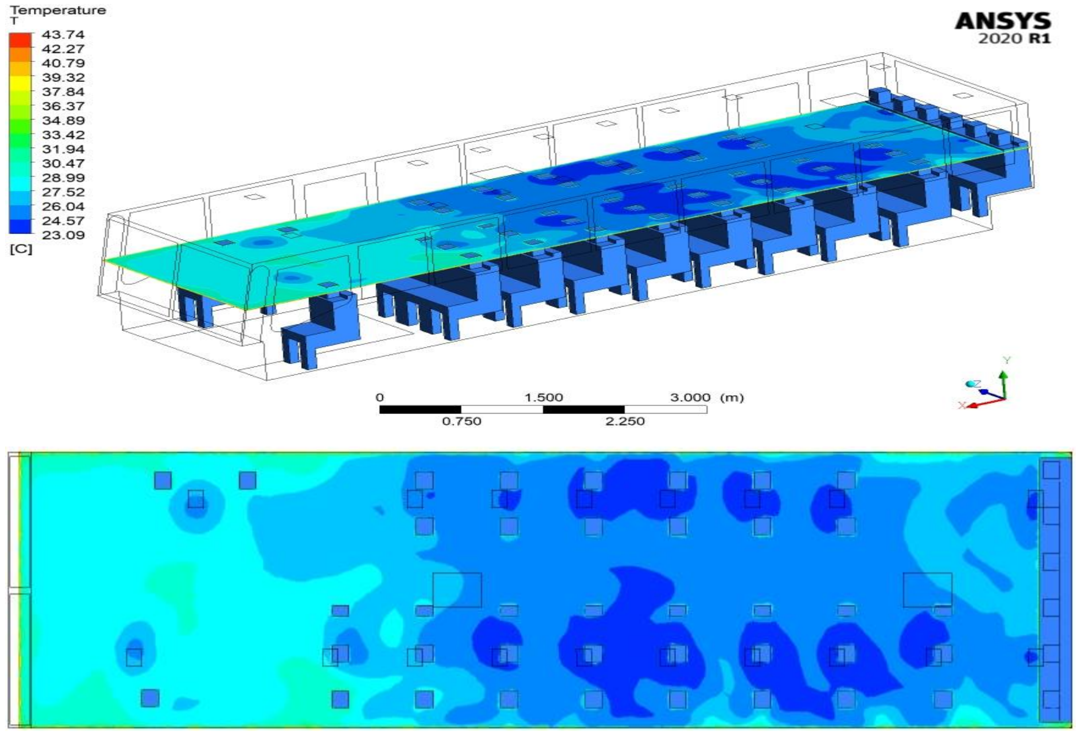

Figure 5.6. Temperature contour plot at passenger head on X-Z plane, at Y = 1.1m

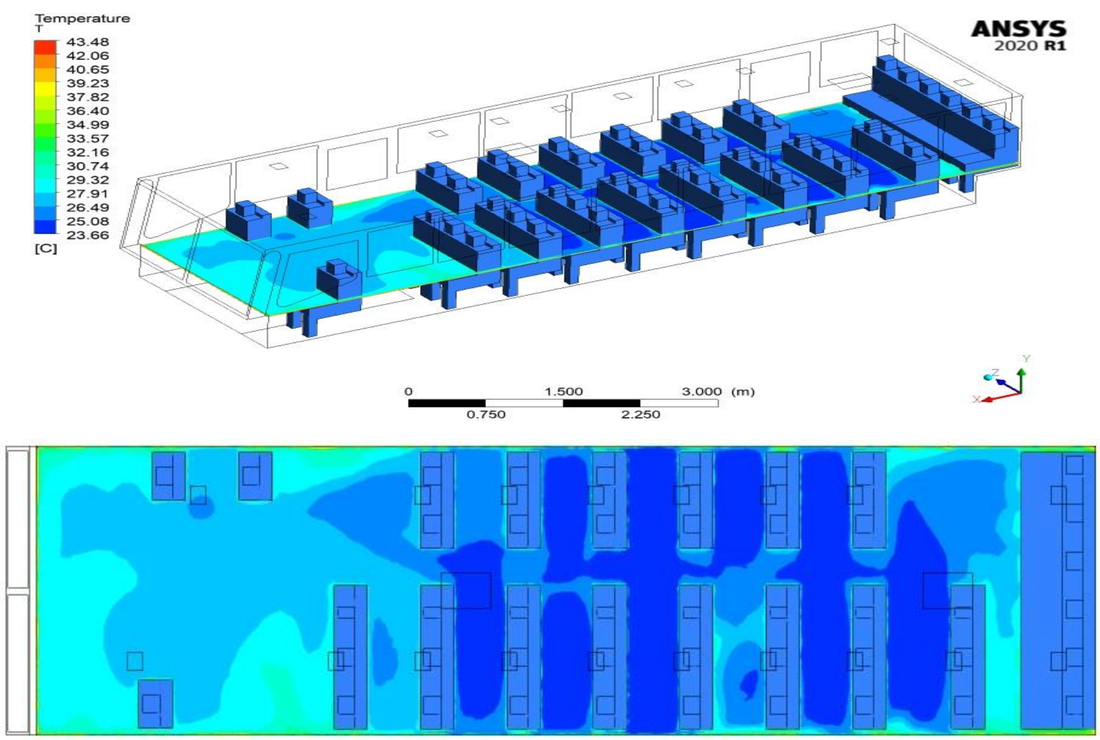

Figure 5.7. Temperature contour plot at passenger knee on X-Z plane, at Y = 0.6 m

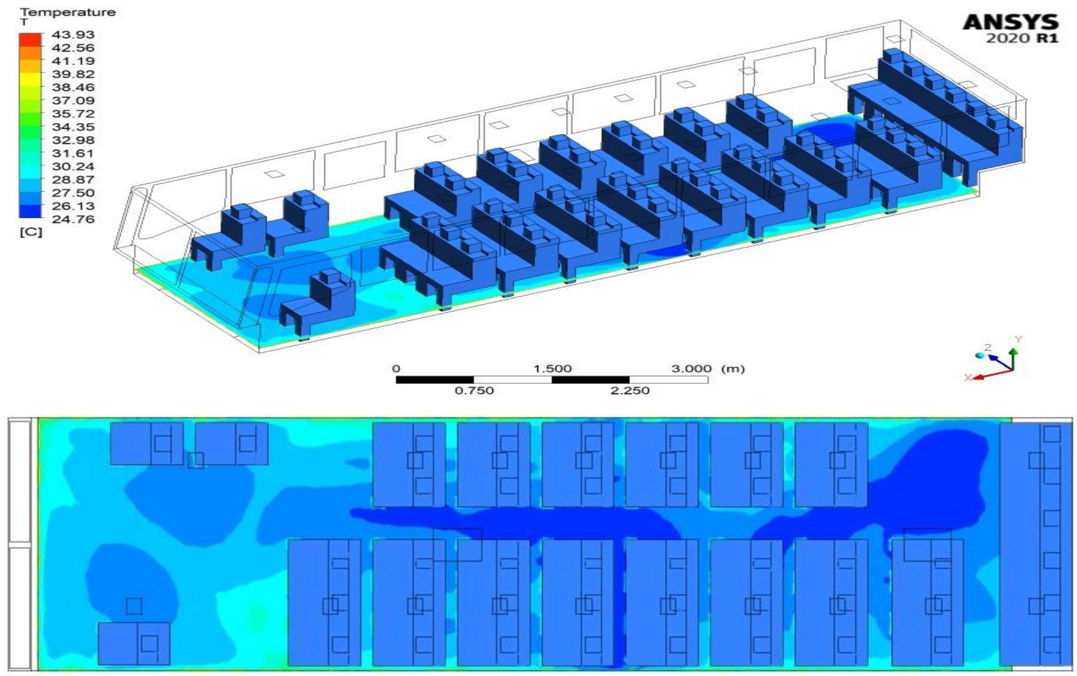

Figure 5.8. Temperature contour plot at passenger ankle on X-Z plane, at Y = 0.1m

As shown from Figure 5.6 to Figure 5.8, the temperature distribution reaches almost all corners of the bus by providing proper thermal comfort. High air temperature was present close to the floor, primarily because of the poor air circulation under the passenger seat. The same high temperature was also shown close to the front windshield driver's space and at rear door free space.

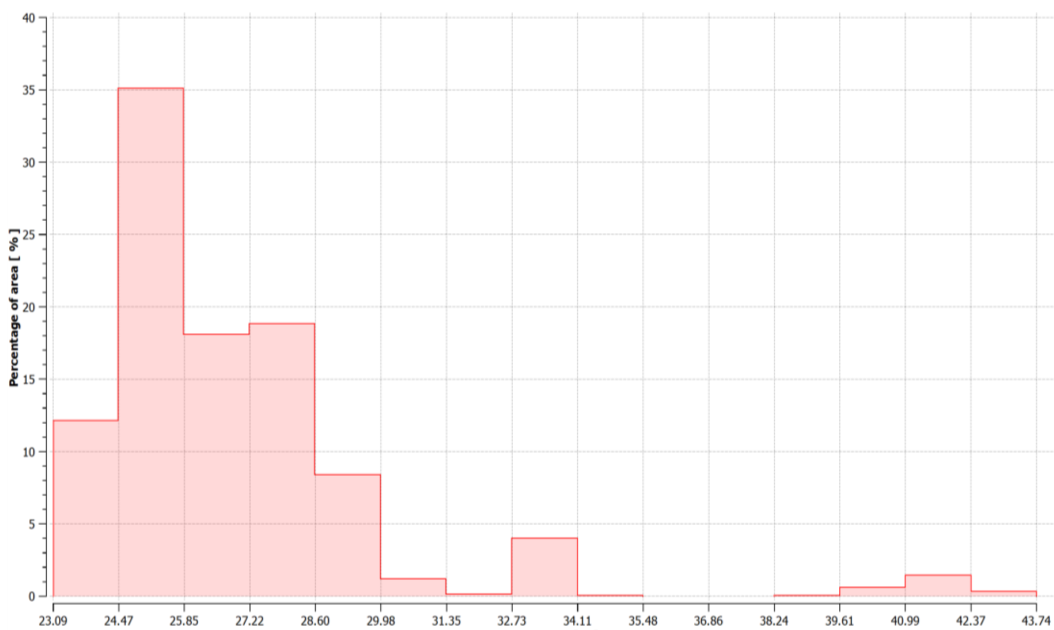

Figure 5.9. Temperature distribution (Plane A).

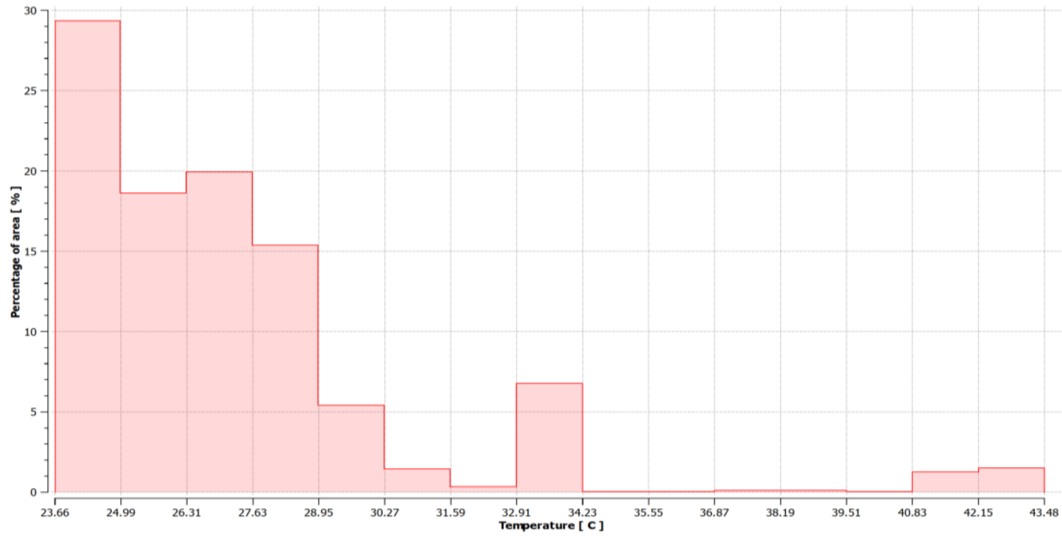

Figure 5.10. Temperature distribution (Plane B).

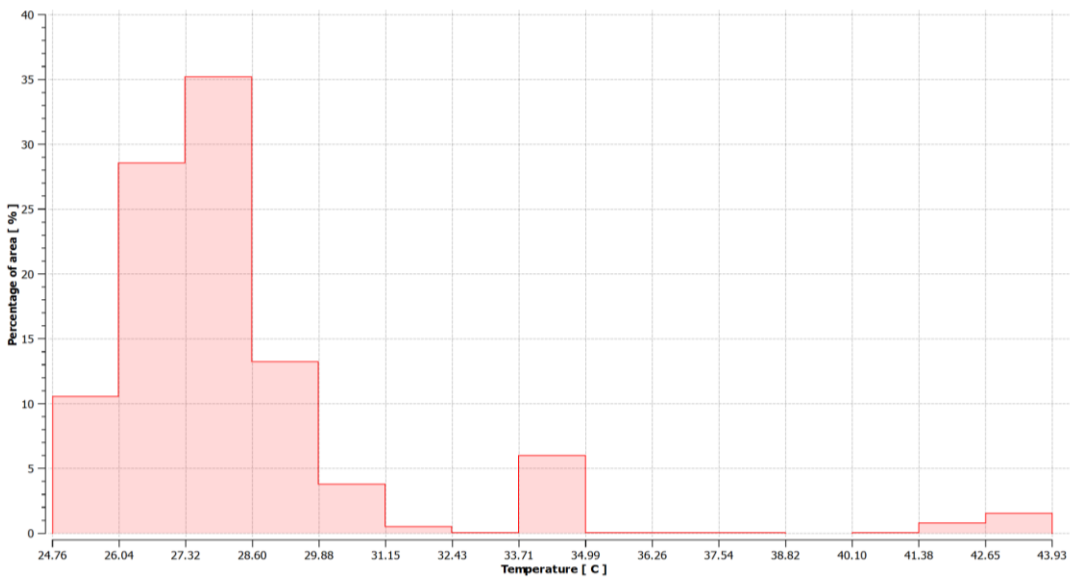

Figure 5.11. Temperature distribution (Plane C).

Figure 5.6 to Figure 5.11 presents the air temperature distribution at plane A to C. The minimum air temperature at the ankles level was 23.09°C, 23.66°C at the sitting person's knee level (0.6m), and 24.76°C at the sitting person's head.

ASHRAE Standard 55 (2004, 2017), prescribes 3°C as the limit for the vertical air temperature difference between head and ankle levels for seated occupants. As shown in the Figure 5.6 and Figure 5.8 above the difference between head and ankle level is below 3°C.

The temperature at the contour planes inside the bus compartment clipped between 23.5°C and 27.78°C which is the common accepted range defined by ASHRAE Standard 55-2004.

5.1.2 Distribution of air velocity

In Figure 5.12 and Figure 5.13 streamlines are illustrating the flow pattern in the passenger compartment. We see how the air circulates entire bus. The velocity distribution is nearly uniform in entire bus passenger compartment except below around passenger legs. The flow behavior inside the compartment has been shown below which is characterized by the flow discharged from air diffusers at angle of 90^o with respect to roof.

Near the inlet area airflow is faster, which is helpful for ventilation. But air velocity away from the inlet area is weak.

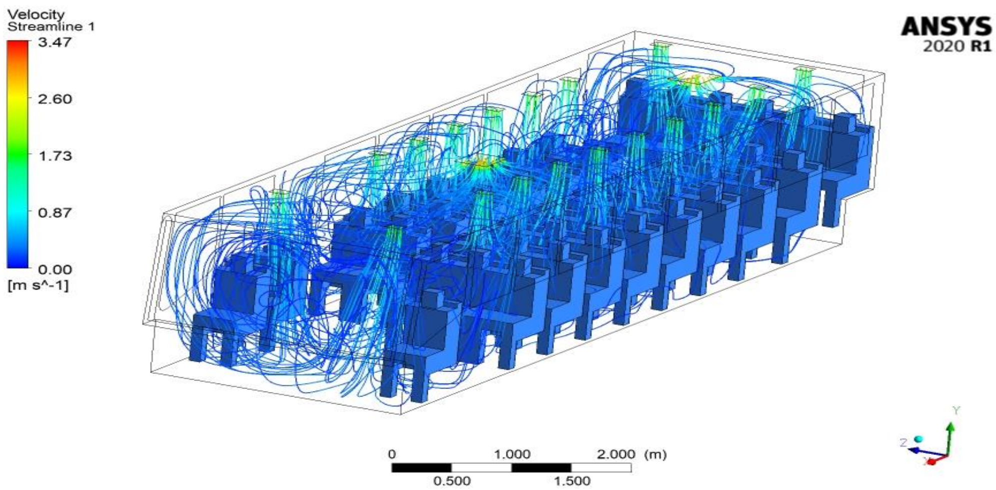

Figure 5.12. Velocity streamlines showing supply air velocity and direction.

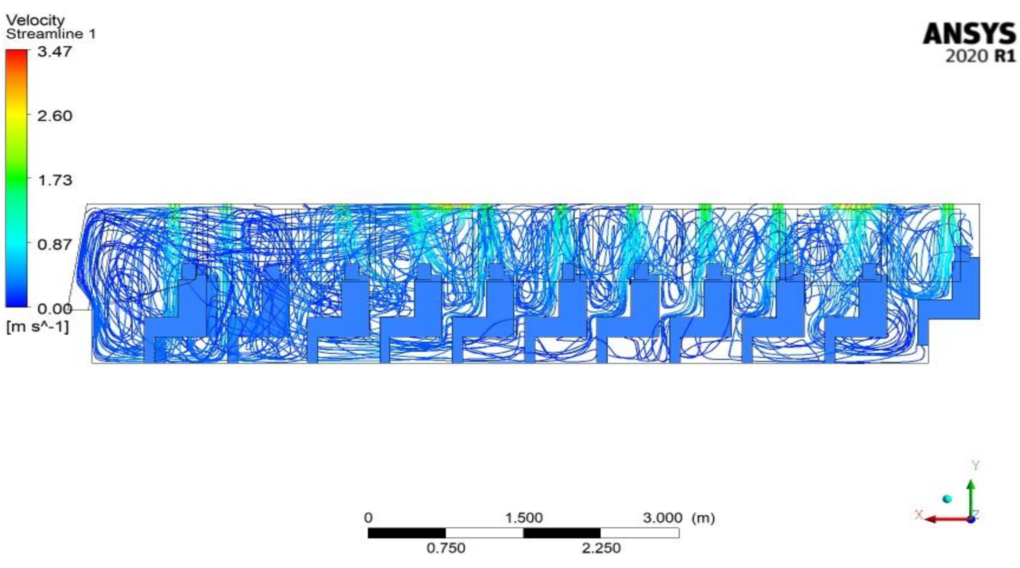

Figure 5.13. Velocity streamline viewed from side.

As we can see from Figure 5.14 and Figure 5.15 the air flow from inlets in one direction and suddenly expand to fill the whole passenger compartment. A lack of flow has been observed near the corners and the lower parts under passenger seat.

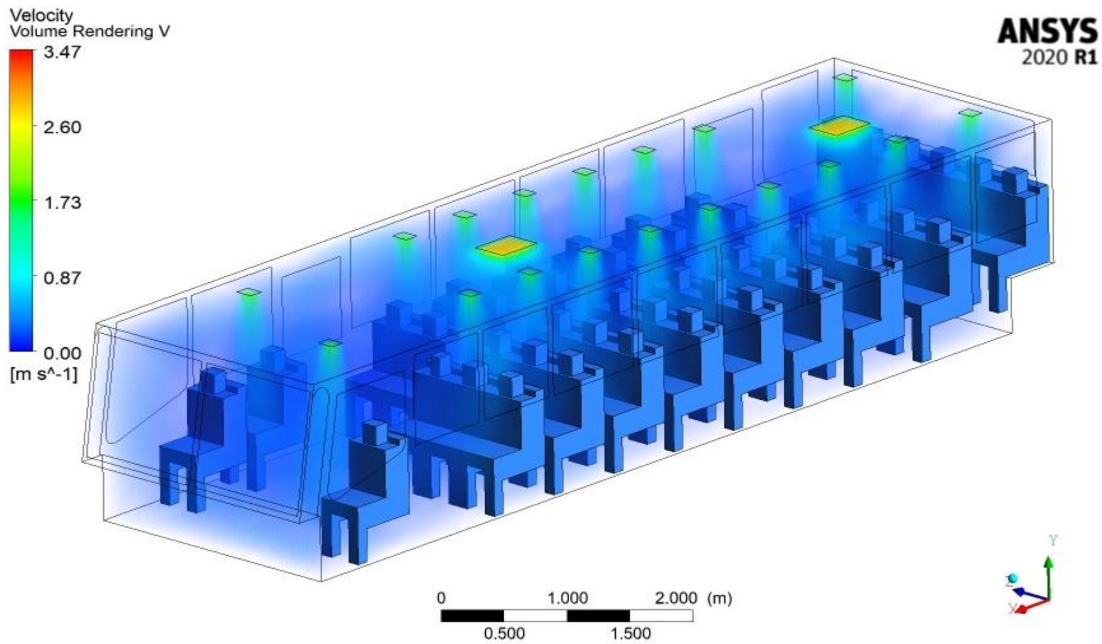

Figure 5.14. Velocity volume rendering.

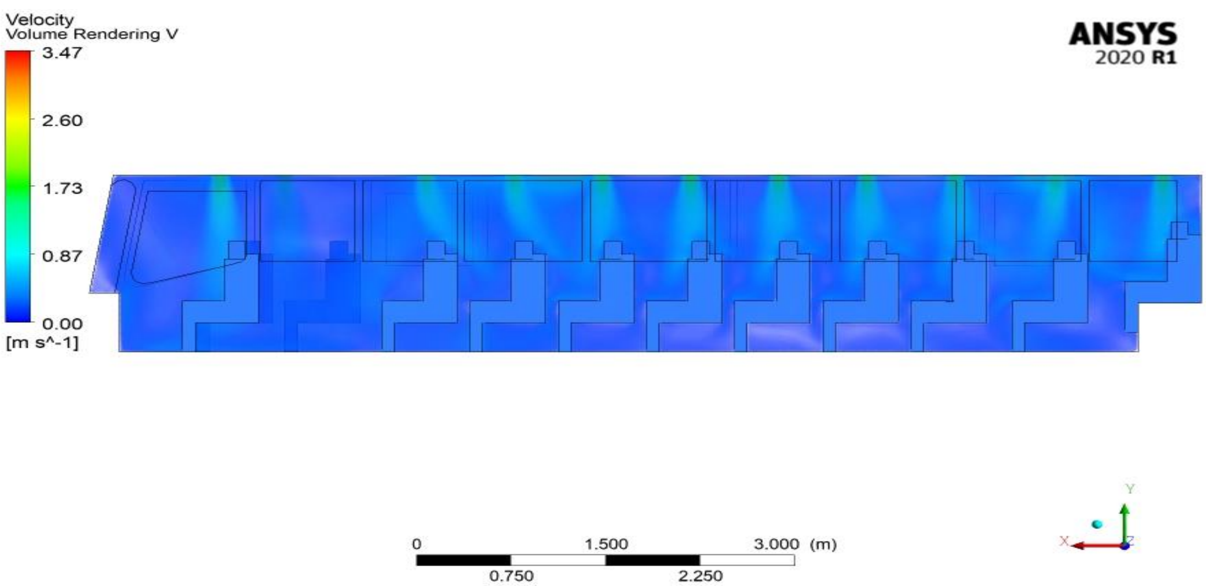

Figure 5.15. Velocity volume rendering viewed from side.

Figure 5.16 shows velocity field magnitude for inlet speed of 1.8293 m/s and outlet speed with a range from 0 m/s to 3.47 m/s.

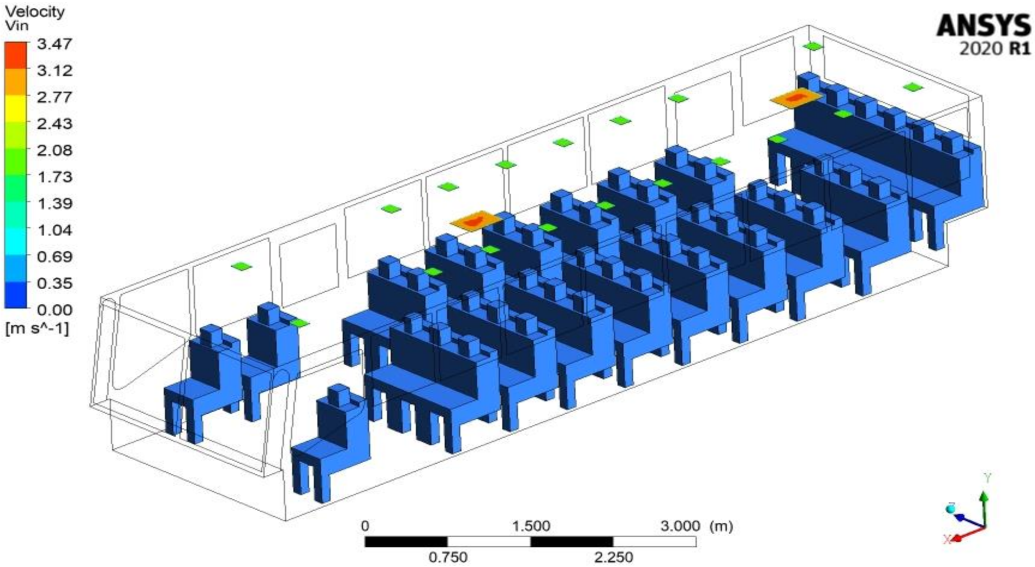

Figure 5.16 Velocity at the inlet and outlet

As expected, the highest airflow velocity occurs at the inlets. The inlet air distributed once it reaches the floor of the bus as evidenced by the contour plots in Figure 5.17 to 5.19. It can also be seen that the flow velocity decreases at the front and around rear door of the bus resulting in low distribution of inlet air at these locations.

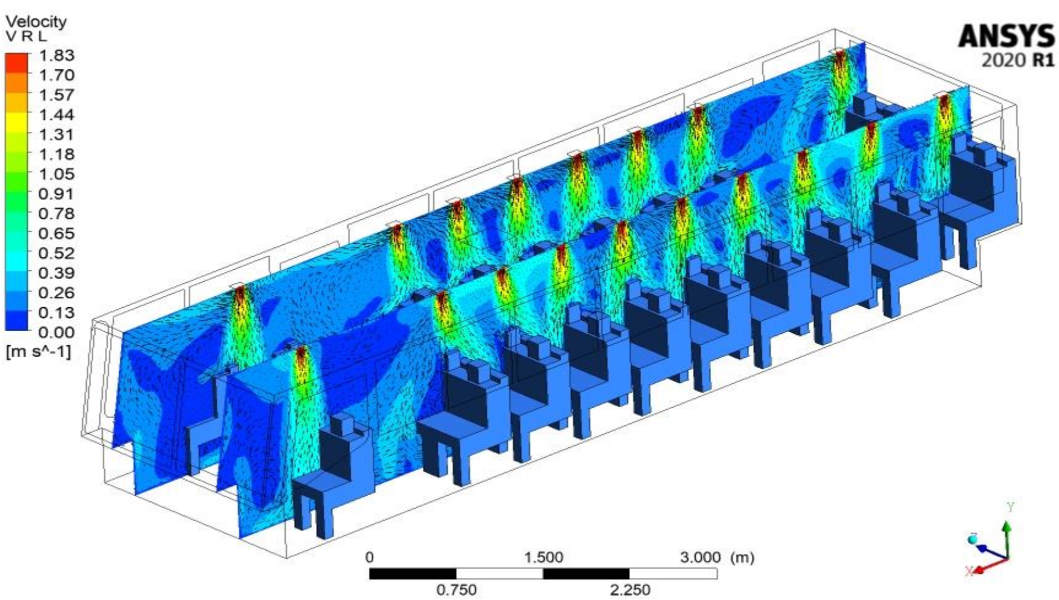

Figure 5.17. velocity profile at inlets

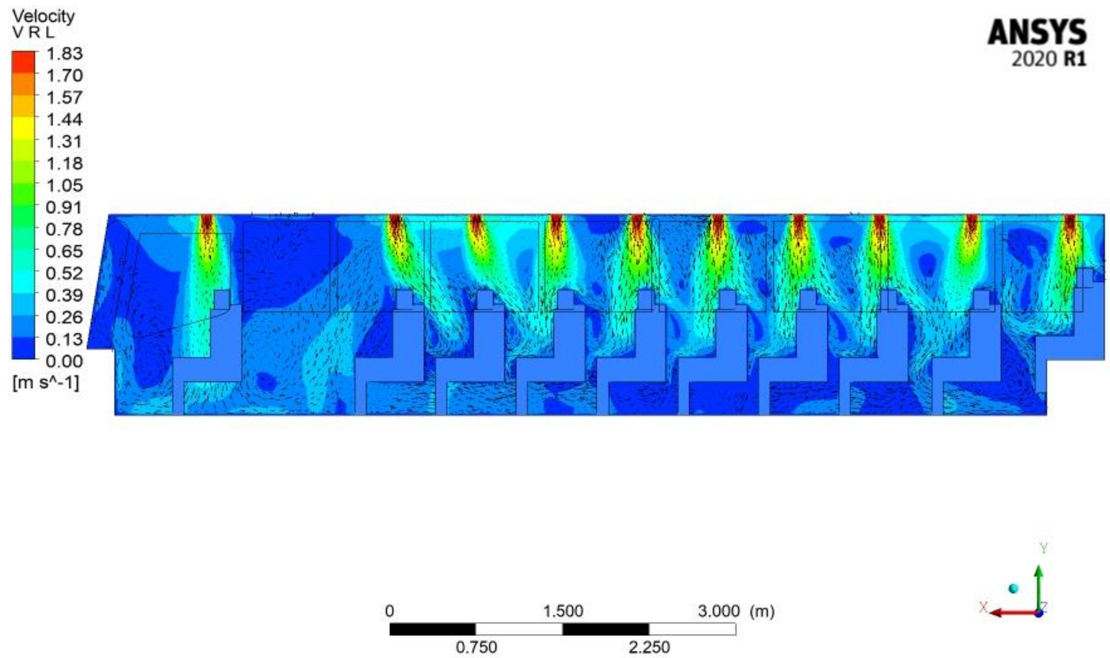

Figure 5.18. velocity profile at left hand side inlets.

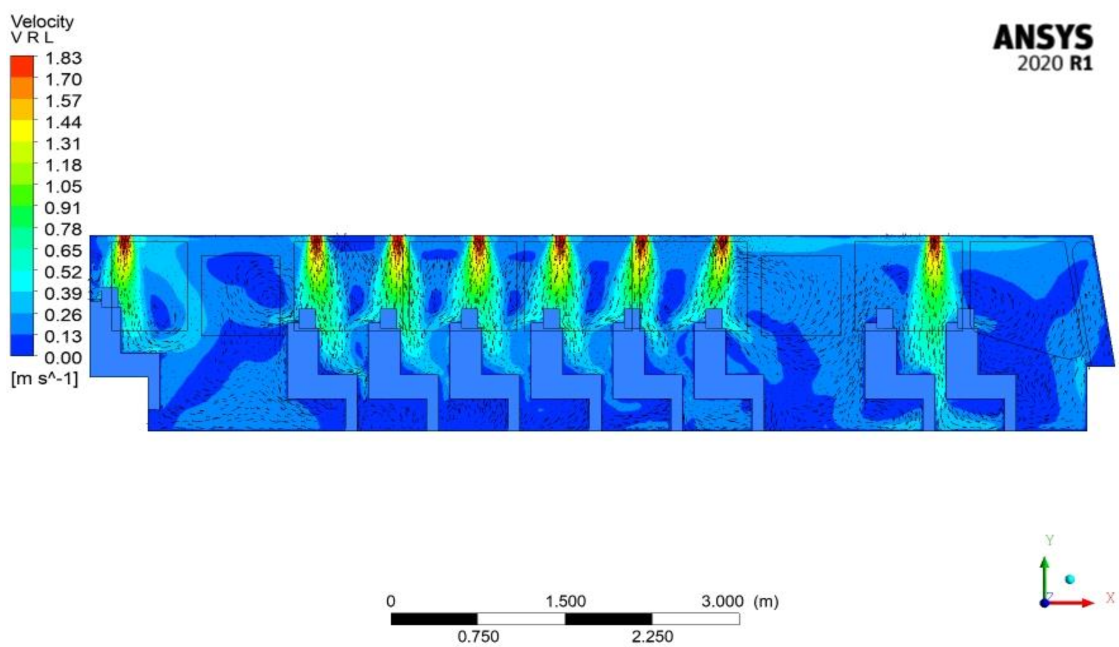

Figure 5.19. velocity profile at right hand side inlets.

Figure 5.20 to Figure 5.22 shows the result of air velocity from plane A to C. As shown in Figure 5.20 higher air velocities in the bus compartment were experienced in area above the simulated person. Figure 5.20 shows that the velocity of air at passenger level is almost 0.8 m/s. It is well within the comfortable zone of the passengers (Petrone et al., 2008). The value has the support of the other researchers (Yongson et al., 2007).

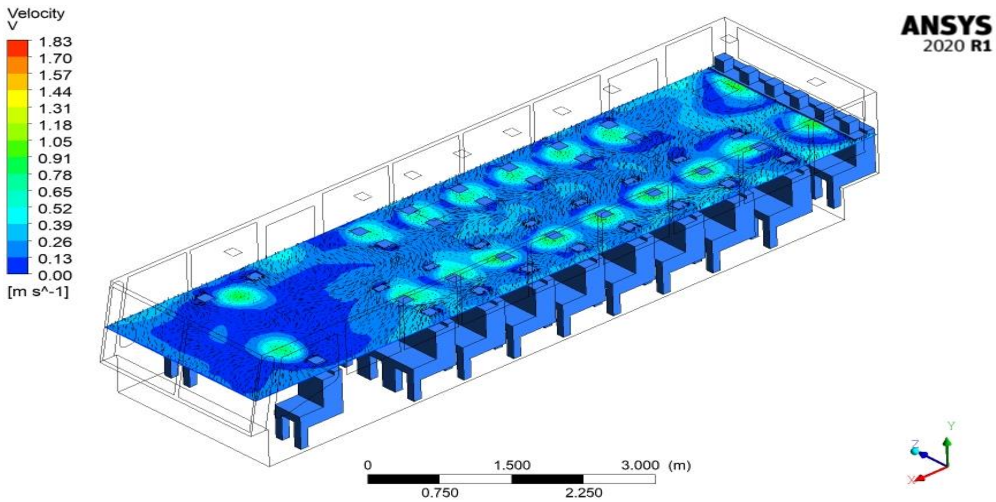

Figure 5.20. Air velocity distribution at plane A.

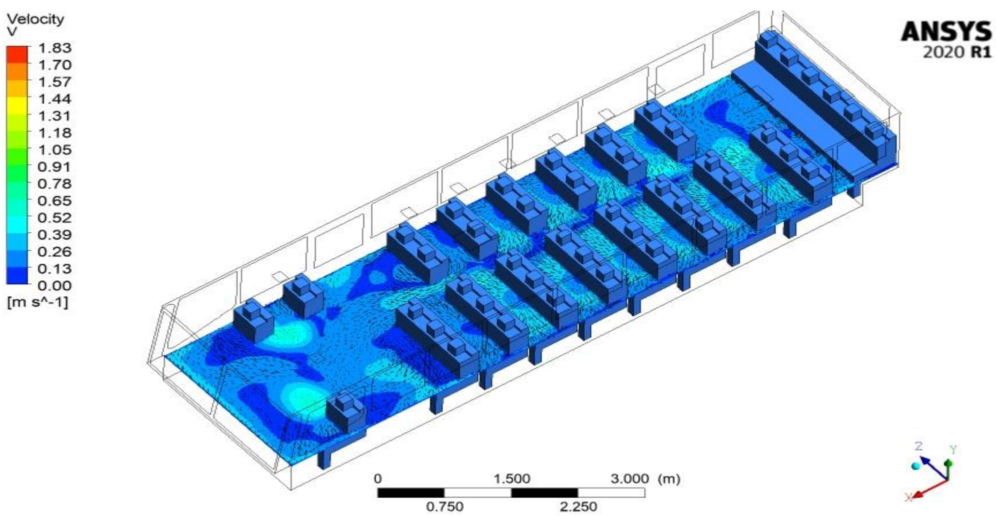

Figure 5.21. Air velocity distribution at plane B.

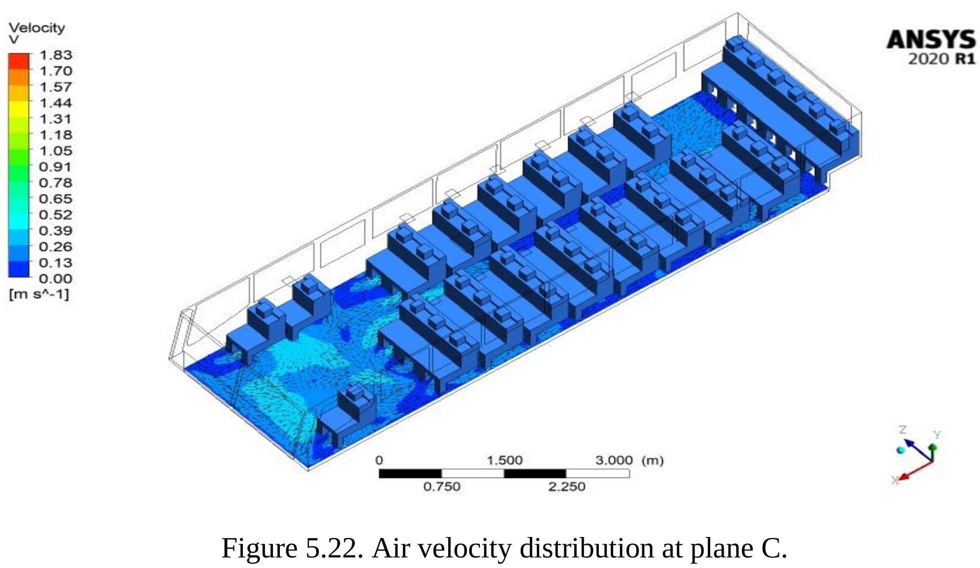

Figure 5.22. Air velocity distribution at plane C.

CHAPTER SIX

CONCULUSION AND RECOMMENDATIONS

6.1 Summary

The goal of this thesis was designing of air conditioning system for locally body-built bus by considering different heat loads and working environment. Firstly, ISUZU FSR local body-built bus with a passenger capacity of 44 people was selected and then heat loads calculated from glass, solid walls, occupant, and engine by considering total number of passengers, outside air conditions, size and optical properties of windows, thermal properties of materials used, and dimensions of the bus body. the method used in calculating the cooling load is the heat balance method. As per the calculations total cooling load and air flow required to the passenger compartment is 26.08kW and 1080L/s respectively. The required rooftop air conditioning unit with the design cooling capacity and air flow for the passenger compartment is selected. To provide equal distribution of conditioned air to passenger compartment duct designed with 18 inlet diffusers and 2 outlets.

The last and most important part of this thesis dealt with CFD analysis to investigate the air flow distribution in the interior of the passenger compartment. 3D model bus was made in SolidWorks and ANSYS Design Modeler to provide stable calculation. The bus actual size is used in the analysis. Mesh structure is formed by polyhedral element structure. The system air flow distribution inside passenger's compartment simulated using ANSYS Fluent 2020 R1, with turbulence model of the shear-stress transport SST $k - \omega$ model. Grid dependence test was carried out to make sure that grid resolution has no effect on the outcome.

6.2 Conclusion

To increase thermal comfort in the locally body-built buses air conditioning system designed. The CFD simulation-based model is used to predict air temperature and air velocity distributions in a model bus compartment. As a result, the following conclusions were obtained:

- From the simulation results, the temperature distribution is reaching almost all corners of the bus with minimum air velocity. The results show the designed air conditioning system is capable to ensure satisfactory thermal conditions for the passengers.
- The contours obtained is showing the area at the corners are showing minimum heat dissipation when compare to the area in between. The colored representation is observed clearly to state the conclusion that the temperature at the center of the bus is minimum when compare with the total heat dissipation at corners.
- Cooling load calculation steps and results obtained from this thesis which might be used as input parameters for any similar or different types of buses locally body built. The CFD method used in this thesis is may be used to study temperature distribution and air flow distribution for different car models.
- Upon implementation of this designed air conditioning system on local body-built buses, make them more comfortable and competitive with other imported air-conditioned buses and the country can save money in importation of the buses.

6.3 Limitations

There is a significant limitation in this study that could be addressed in future research. In this study, the Ansys simulation is done considering the worst-case outdoor design temperature with a combination of the bus body's material properties and relevant and reasonable boundary conditions. But it had to be simulated using constant heat flux and solar radiation instead of constant temperature to achieve better results. In addition, heat gain from the engine and exhaust pipe should be simulated using constant heat flux.

6.4 Recommendations

Now a day's people spend a long time in the long-distance transports because of different reason. The idea of air conditioning in transport arises from the need to improve the comfort of the people who use it. For this reason, it is recommended that the local bus body manufacturing companies or garages to include air conditioning system in the new or previously manufactured buses in order to increase the comfort of passengers and driver.

6.5 Future scope of the work

The future researchers who are willing to conduct a similar study to perform calculation using actual data derived from measurement of inside air, wall, floor, and ceiling temperature using thermometer at extreme hot climate location.

Based on both our numerical and simulation result on the bus there is a need to further study on alternate air distribution methods in order to improve the air conditioning efficiency.

The thesis can be extended by varying the different input temperatures.

Further research on methods on vehicle air-conditioning which yield fuel efficiency might be of interest for the willing researchers.

REFERENCES

Akbari, H., Levinson, R., and Berdahl, P. (1996). ASTM standards for measuring solar reflectance and infrared emittance of construction materials and comparing their steady-state surface temperatures. ACEEE, Vol. 1, 1.4- 1.5.

Andre, J.C.S., Conceição, E.Z.E., Silva, M.C.G., and Viegas, D.X. (1994). Integral simulation of air conditioning in passenger buses. Fourth International Conference on Air Distribution in Rooms (ROOMVENT ’94).

ASHRAE Handbook Fundamentals (1997). Atlanta, Georgia. American Society of Heating, Refrigerating and Air-conditioning Engineers.

ASHRAE Handbook Fundamentals (2017). Atlanta, Georgia. American Society of Heating, Refrigerating and Air-conditioning Engineers.

ASHRAE Handbook HVAC (2019). Atlanta, Georgia. American Society of Heating, Refrigerating and Air-conditioning Engineers.

ASHRAE Standard 55. (2004). Thermal environmental conditions for human occupancy. ANSI/ASHRAE Standard 55-2004. Atlanta, Georgia. American Society of Heating, Refrigerating and Air-conditioning Engineers.

ASHRAE Standard 55. (2017). Thermal environmental conditions for human occupancy. ANSI/ASHRAE Standard 55-2017. Atlanta, Georgia. American Society of Heating, Refrigerating and Air-conditioning Engineers.

ANSYS. (2020). Ansys Fluent Features. Retrieved January 10, 2021, from https://www.ansys.com/products/fluids/ansys-fluent/ansys-fluent-features

ANSYS Fluent 12.0. (2009). Turbulence modeling. Retrieved January 10, 2021, from https://www.afs.enea.it/project/neptunius/docs/fluent/html/th/node57.htm

Berlitz, T., and Matschke, G. (2004). Interior Airflow Simulation in Railway Rolling Stock. Research and Technology Centre of the Deutsche Bahn AG, Division for Aerodynamics and Air-conditioning, FTZ, Völckerstraße 5, 80939 München.

Bhargava, S.C. (2020). Household Electricity and Appliances. BSP Books Pvt., Ltd., 4-4-309/316, Giriraj Lane, Sultan Bazar, Hyderabad.

Bhatia, A. (2010). HVAC- How size and design ducts. Retrieved April 10, 2020 from https://www.cedengineering.com/userfiles/HVAC-HowSizeandDesignDuctsR1.pdf.

Cengel, Y.A., and Boles, M.A. (2010). Thermodynamics an Engineering Approach. 5th Edition.

Climate-Data.org. (2020). Semera Climate. Retrieved August 11, 2020, from https://en.climate-data.org/africa/ethiopia/afar/semera-55037/

Dayton ASHRAE Online Psychrometric (2020). Psychrometric Properties SI Units. Retrieved April 10, 2020, from https://daytonashrae.org/psychrometrics/psychrometrics_si.html#start

EBCS 11(2014). Mechanical Ventilation and Air conditioning in Buildings. Ethiopian Building Code Standard.

GUCHEN. (2015). Bus HVAC- Bus air conditioning Catalog. Retrieved April 10, 2020, from https://www.guchen.com/bus-air-conditioner/bus-hvac-solutions.html.

Ingersoll, J., Kalman, T., Maxwell, L., and Niemiec, R., (1992). Automobile Passenger Compartment Thermal Comfort Model - Part I: Compartment Cool-Down/Warm-Up Calculation. SAE Technical Paper 920265.

Jordan, R.C., and Prester, G.B. (1969). Refrigeration and Air Conditioning. Second edition. Pergamon Press Ltd., Headington Hill Hall, Oxford.

Khayyam, H., Kouzani, A.Z., and Hu, E.J. (2009). Reducing Energy Consumption of Vehicle Air Conditioning System By a Energy Management System. IEEE Intelligent Vehicles Symposium, IEEE, Piscataway, N. J., pp. 752-757.

Mezrhab, A., and Bouzidi, M. (2006). Computation of Thermal Comfort Inside a Passenger Car Compartment. Applied Thermal Engineering. Vol, 26. pp. 1697- 1704.

Rugh, J.P., and Bharathan, B. (2005). Predicting Human Thermal Comfort in Automobiles. SAE Technical Paper 10.2172/15016823.

Petrone, G., Fichera, G., and Scionti, M. (2008). Thermal and Fluid-dynamical Optimisation of Passengers Comfort in a Touring Bus Cabin. Departement of Industrial and Mechanical Engineering, University of Catania. Italy.

Pirouz, B., Mazzeo, D., Palermo, S.A., Naghib, S.N., Turco, M., and Piro, P. (2021). CFD Investigation of Vehicle’s Ventilation Systems and Analysis of ACH in Typical Airplanes, Cars, and Buses. Sustainability, 13, 6799.

Soliman, M.H.A. (2020). Industrial Applications of Infrared Thermography. Retrieved from https://books.google.com.et/books?id=uf0qEAAAQBAJ&printsec=frontcover#v=onepage&q&f=false

Vollaro, R.D.L. (2013). Indoor Climate Analysis for Urban Mobility Buses: A CFD Model for the Evaluation of Thermal Comfort. International Journal of Environmental Protection Policy. Department Engineering of University of Rome. Italy. Vol. 3, No. 1.

Weather spark (2020). Average weather in Semera. Retrieved August 11, 2020, from https://weatherspark.com/td/101920/Average-Weather-in-Semera-Ethiopia-Today

Yongson, O., Badruddin, A.B., Zainal, Z.A., and Narayana, P.A.A. (2007). Airflow Analysis in an Air Conditioning Room. Building and Environment, 42, 1531–1537.

You, R., Zhang, Y., Zhao, X., Lin, C., Wei, D., Liu, J., and Chen, Q. (2018). An Innovative Personalized Displacement Ventilation System for Airliner Cabins. Building and Environment, 137, 41-50.

Zhai, Z., Zhang, Z., Zhang, W., and Chen, Q. (2007). Evaluation of various turbulence models in predicting airflow and turbulence in enclosed environments by CFD: Part-1: summary of prevent turbulence models,” *HVAC&R Research*, 13(6).

APPENDIX A: DESIGN CONDITION FOR COOLING

Location				Annual cumulative frequency of occurrence (%)											
				0.4				1				2.5[1]			
City/Town	Latitude	Longitude	Elevation	DBT (^{0}C)	CWB (^{0}C)	DPT (^{0}C)	MDR	DBT (^{0}C)	CW B	DPT (^{0}C)	MDR	DBT (^{0}C)	CW B	DPT (^{0}C)	MDR
Adama	08^{0}55'N	38^{0}55'E	1712m	33.9	28.03	21.25	19.7 1	33.5	23.4 3	18.25	19.7 1	32.6	24.5 4	20.82	19.71
Addis Ababa	09^{0}02'N	39^{0}42'E	2355m	29	23.07	20.35	18.4 6	28.5	22.5 9	19.81	18.4 6	28	21.1 9	17.73	18.46
Assosa	10^{0}04'N	34^{0}32'E	1570m	35	22.86	14.56	22.8 4	34.5	21.7	14.16	22.8 4	34	22.9 4	17.02	22.84
Bahirdar	11^{0}37'N	37^{0}10'E	1800m	33	21.48	14.72	23.5 9	32.6	19.7 3	11.3	23.5 9	32.2	21.0 9	14.52	23.59
Dire Dawa	09^{0}35'N	41^{0}45'E	1200m	38.5	25.88	19.8	20.3 1	38	27.4	22.75	20.3 1	37.6	25.9 9	20.53	20.31
Gambella	08^{0}15'N	34^{0}34'E	514m	42.5	29.92	24.92	23.5 0	42	30.0 8	25.38	23.5 0	41.5	29.7 8	25.11	23.50
Gode	05^{0}57'N	43^{0}27'E	254m	39.6	34.78	33.13	17.8 9	39.2	33.9 4	32.1	17.8 9	38.7	33.3 3	31.44	17.89
Jijiga	09^{0}20'N	42^{0} 50'E	1609m	32.5	24.12	20.1	26.7 2	32.2	22.5 3	17.45	26.7 2	31.7	23.6 4	19.72	26.72
Mekelle	13^{0}33'N	39^{0}30'E	2084m	30	27.97	27.18	18.9 5	29.8	27.4 8	26.57	18.9 5	29.4	27.2 8	26.44	18.95
Semera	11^{0}30'N	41^{0} 12'E	633m	44.5	28.71	21.81	25.8 5	44	28.6 2	21.99	25.8 5	43.8	31.6 5	27.1	25.85

APPENDIX B: CIRCULAR EQUIVALENTS OF RECTANGULAR DUCT

Lgth Adj.[b]	Length of One Side of Rectangular Duct (a), mm																			
	100	125	150	175	200	225	250	275	300	350	400	450	500	550	600	650	700	750	800	900
	Circular Duct Diameter, mm																			
100	109																			
125	122	137																		
150	133	150	164																	
175	143	161	177	191																
200	152	172	189	204	219															
225	161	181	200	216	232	246														
250	169	190	210	228	244	259	273													
275	176	199	220	238	256	272	287	301												
300	183	207	229	248	266	283	299	314	328											
350	195	222	245	267	286	305	322	339	354	383										
400	207	235	260	283	305	325	343	361	378	409	437									
450	217	247	274	299	321	343	363	382	400	433	464	492								
500	227	258	287	313	337	360	381	401	420	455	488	518	547							
550	236	269	299	326	352	375	398	419	439	477	511	543	573	601						
600	245	279	310	339	365	390	414	436	457	496	533	567	598	628	656					
650	253	289	321	351	378	404	429	452	474	515	553	589	622	653	683	711				
700	261	298	331	362	391	418	443	467	490	533	573	610	644	677	708	737	765			
750	268	306	341	373	402	430	457	482	506	550	592	630	666	700	732	763	792	820		
800	275	314	350	383	414	442	470	496	520	567	609	649	687	722	755	787	818	847	875	
900	289	330	367	402	435	465	494	522	548	597	643	686	726	763	799	833	866	897	927	984
1000	301	344	384	420	454	486	517	546	574	626	674	719	762	802	840	876	911	944	976	1037
1100	313	358	399	437	473	506	538	569	598	652	703	751	795	838	878	916	953	988	1022	1086
1200	324	370	413	453	490	525	558	590	620	677	731	780	827	872	914	954	993	1030	1066	1133
1300	334	382	426	468	506	543	577	610	642	701	757	808	857	904	948	990	1031	1069	1107	1177
1400	344	394	439	482	522	559	595	629	662	724	781	835	886	934	980	1024	1066	1107	1146	1220
1500	353	404	452	495	536	575	612	648	681	745	805	860	913	963	1011	1057	1100	1143	1183	1260
1600	362	415	463	508	551	591	629	665	700	766	827	885	939	991	1041	1088	1133	1177	1219	1298
1700	371	425	475	521	564	605	644	682	718	785	849	908	964	1018	1069	1118	1164	1209	1253	1335
1800	379	434	485	533	577	619	660	698	735	804	869	930	988	1043	1096	1146	1195	1241	1286	1371
1900	387	444	496	544	590	663	674	713	751	823	889	952	1012	1068	1122	1174	1224	1271	1318	1405
2000	395	453	506	555	602	646	688	728	767	840	908	973	1034	1092	1147	1200	1252	1301	1348	1438
2100	402	461	516	566	614	659	702	743	782	857	927	993	1055	1115	1172	1226	1279	1329	1378	1470
2200	410	470	525	577	625	671	715	757	797	874	945	1013	1076	1137	1195	1251	1305	1356	1406	1501
2300	417	478	534	587	636	683	728	771	812	890	963	1031	1097	1159	1218	1275	1330	1383	1434	1532
2400	424	486	543	597	647	695	740	784	826	905	980	1050	1116	1180	1241	1299	1355	1409	1461	1561
2500	430	494	552	606	658	706	753	797	840	920	996	1068	1136	1200	1262	1322	1379	1434	1488	1589
2600	437	501	560	616	668	717	764	810	853	935	1012	1085	1154	1220	1283	1344	1402	1459	1513	1617
2700	443	509	569	625	678	728	776	822	866	950	1028	1102	1173	1240	1304	1366	1425	1483	1538	1644
2800	450	516	577	634	688	738	787	834	879	964	1043	1119	1190	1259	1324	1387	1447	1506	1562	1670
2900	456	523	585	643	697	749	798	845	891	977	1058	1135	1208	1277	1344	1408	1469	1529	1586	1696

APPENDIX C: FITTING LOSS COEFFICIENT

SR5-13 Tee, 45 Degree Entry Branch, Diverging

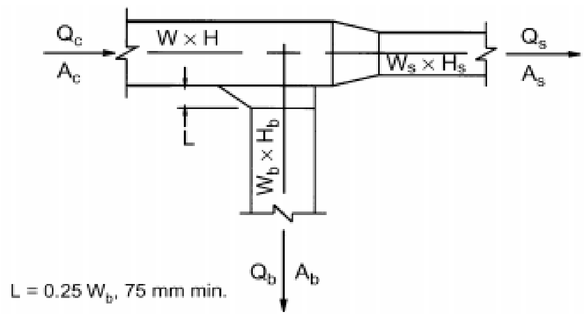

	C_b Values								
	Q_b/Q_c								
A_b/A_c	0.1	0.2	0.3	0.4	0.5	0.6	0.7	0.8	0.9
0.1	0.73	0.34	0.32	0.34	0.35	0.37	0.38	0.39	0.40
0.2	3.10	0.73	0.41	0.34	0.32	0.32	0.33	0.34	0.35
0.3	7.59	1.65	0.73	0.47	0.37	0.34	0.32	0.32	0.32
0.4	14.20	3.10	1.28	0.73	0.51	0.41	0.36	0.34	0.32
0.5	22.92	5.08	2.07	1.12	0.73	0.54	0.44	0.38	0.35
0.6	33.76	7.59	3.10	1.65	1.03	0.73	0.56	0.47	0.41
0.7	46.71	10.63	4.36	2.31	1.42	0.98	0.73	0.58	0.49
0.8	61.79	14.20	5.86	3.10	1.90	1.28	0.94	0.73	0.60
0.9	78.98	18.29	7.59	4.02	2.46	1.65	1.19	0.91	0.73

	C_s Values								
	Q_s/Q_c								
A_s/A_c	0.1	0.2	0.3	0.4	0.5	0.6	0.7	0.8	0.9
0.1	0.04								
0.2	0.98	0.04							
0.3	3.48	0.31	0.04						
0.4	7.55	0.98	0.18	0.04					
0.5	13.18	2.03	0.49	0.13	0.04				
0.6	20.38	3.48	0.98	0.31	0.10	0.04			
0.7	29.15	5.32	1.64	0.60	0.23	0.09	0.04		
0.8	39.48	7.55	2.47	0.98	0.42	0.18	0.08	0.04	
0.9	51.37	10.17	3.48	1.46	0.67	0.31	0.15	0.07	0.04

CR3-9 Elbow, Mitered, 90 Degree, Single-Thickness Vanes (Design 1)

$C_o = 0.11$